A Generic Theory of the Integer Quantum Hall Effect

Yu Shen

A Dissertation
Presented to the Faculty
of Princeton University
in Candidacy for the Degree
of Doctor of Philosophy

Recommended for Acceptance
by the Department of
Physics
Adviser: Professor F. D. M. Haldane

September 2017

Abstract

The integer quantum Hall effect (IQHE) is usually modeled by a Galilean or rotationally invariant Hamiltonian. These are not generic symmetries for electrons moving in a crystal background and can potentially confuse non-topological quantities with topological ones and identify otherwise distinct geometrical properties. In this thesis we present a generic theory for the IQHE. First we show that a generic guiding-center coherent state, defined by a natural metric in each Landau level, has the form of an antiholomorphic function times an exponential factor. Then by numerically solving the eigen problem for a quartic Hamiltonian and finding the roots of the antiholomorphic part we are able to define a topological spin $s_n = n + \frac{1}{2}$ where n is the number of central roots that are enclosed by the semiclassical orbit. We derive a generic formula for the Hall viscosity in the absence of rotational symmetry and show that the previous interpretation of the scalar Hall viscosity as the "intrinsic orbital angular momentum" breaks down since the concept of angular momentum requires the presence of rotational symmetry. We also calculate generic electromagnetic responses and differentiate between universal terms that are diagonal with respect to Landau level index and non-universal terms that depend on inter-Landau-level mixing. We conclude that the generic theory offers a fundamental definition for the topological spin and reveals finer structure in the geometrical properties of the IQHE.

Acknowledgements

The past five years have been one of the most unforgettable chapters in my life. I feel so lucky and honored to be able to work with Prof. F. D. M. Haldane, one of the greatest physicists in the world, who has taught me what the true beauty of physics is. I have always been influenced by his unfading enthusiasm for and unique perspectives on physical problems. Besides, my research would not have gone as smoothly without so many enlightening discussions with my colleagues Bo Yang, Yeje Park and Jie Wang.

Theorist as I am, I had an opportunity to put on my experimentalist hat during the first summer in Princeton thanks to the generous support by Prof. Robert Austin. I still remember his jocular personality and lighthearted remark—you are indeed a theorist. During the last summer, I had an enjoyable collaboration with Yun Tao Bai to build a course website for Prof. Steven Gubser, who also provided tremendous help to my job-hunting.

When I first came to Princeton, I met so many wonderful people—Jingke Xu, Yangle Wu, Jun Xiong, Bo Zhao, Chaney Lin and Liangsheng Zhang, who offered me helpful advice on how to "survive" in Princeton. I went through various departmental requirements together with the friends in my cohort—Bin Xu, Suerfu, Ilya Belopolski, Sarthak Parikh, Lin Fei and Grigory Tarnopolsky. As I became a senior student, I still learned so much from the junior students—Wudi Wang, Huan He, Yunqin Zheng, Zhenbin Yang, Jingyu Luo, Zheng Ma, Xue Song, Jiaqi Jiang and Junyi Zhang about their passion for both physics and life. I must not forget to thank my five-year roommate, Duyu Chen, an extremely nice person to live with.

I would like to thank Bijie Qiu. I am a better person because of you. I am grateful for the part of your life you shared with me.

This acknowledgment would be incomplete without expressing my deepest gratitude to my parents, who have been supporting me with their unconditional love wherever I am, whatever I do. I live for myself, and for them.

Presentations and Publications

The content in Chap.(2) and Chap.(3) was presented in the APS March Meeting 2016 under the title "Geometry of Landau levels without Galilean or rotational symmetry" and the content in Chap.(4) and Chap.(5) was presented in the APS March Meeting 2017 under the title "Generic Hall viscosity and response functions in the IQHE".

Most of the content in this dissertation, co-authored with F.D.M. Haldane, was submitted to arXiv[21] and Physical Review B.

To my parents.

Contents

Chapter 1

Introduction

In this chapter an overview of the integer quantum Hall effect (IQHE) will be provided. The usual theoretical treatment in the literature where the single-particle Hamiltonian has a quadratic dispersion will be reviewed in detail in order to see both its achievements and limitations. We argue that Galilean symmetry and the more general rotational symmetry are not generic symmetries of electrons moving in a crystal background. The goal of this thesis is then to present a generic theory for the IQHE without these special symmetries.

1.1 IQHE

The quantum Hall effect (QHE) has been a field of active research since the monumental discovery of the integer case by Klitzing *et al.* in 1980[26]. The phenomenon is demonstrated by a two-dimensional electron gas (2DEG) under a constant magnetic field that is perpendicular to the 2D plane. A 2DEG can be realized at the surface of a semiconductor (like Si or GaAs) in contact with an insulating material (SiO_2 for Si and $Al_xGa_{1-x}As$ for GaAs). Electrons are confined to the surface by an electrostatic field normal to the surface. For electrical measurements on a 2DEG, heavily doped n^+ (the plus sign standing for "heavily doped") contacts are used as current and

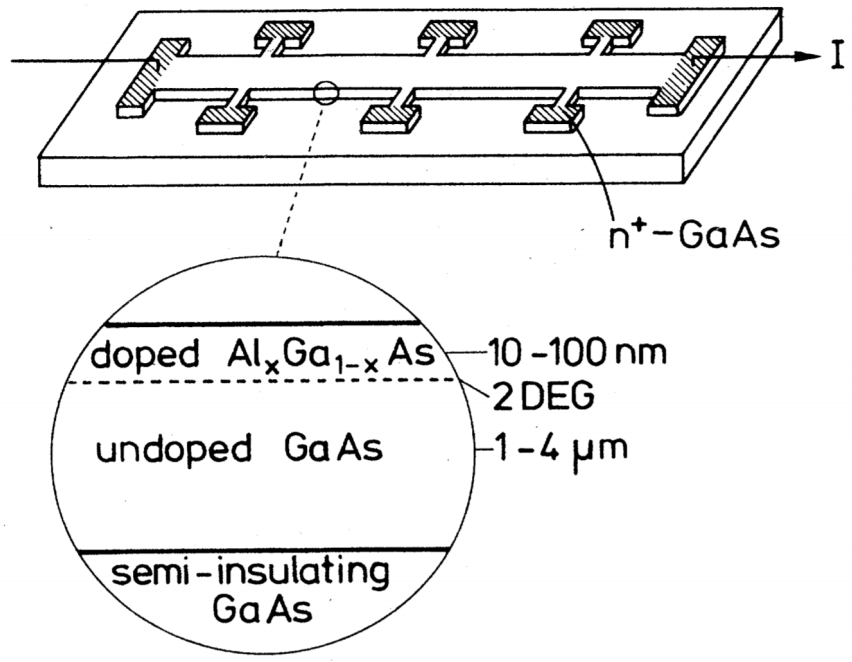

Figure 1.1: Typical configuration and cross section of a GaAs-$Al_xGa_{1-x}As$ heterostructure used for Hall-effect measurements[41].

potential probes. A typical sample used for the QHE experiments is shown in Fig. (1.1).

The curve of the off-diagonal element of the conductivity tensor against the magnetic field has the so-called plateaus where it stays at a fixed value (see Fig.(1.2)), which is an integer number ν, called the filling factor, times a physical constant,

$$\sigma_{xy} = \nu \frac{e^2}{h}, \tag{1.1}$$

and dramatic transitions occur between neighboring plateaus with different ν. The diagonal elements of the conductivity tensor are only nonzero within the transitional ranges, i.e., the quantum Hall system is a perfect insulator at the plateaus.

The amazing property of the IQHE is that the quantization of the Hall conductivity is robust to disorders in the system. Laughlin[28] showed that this is guaranteed by

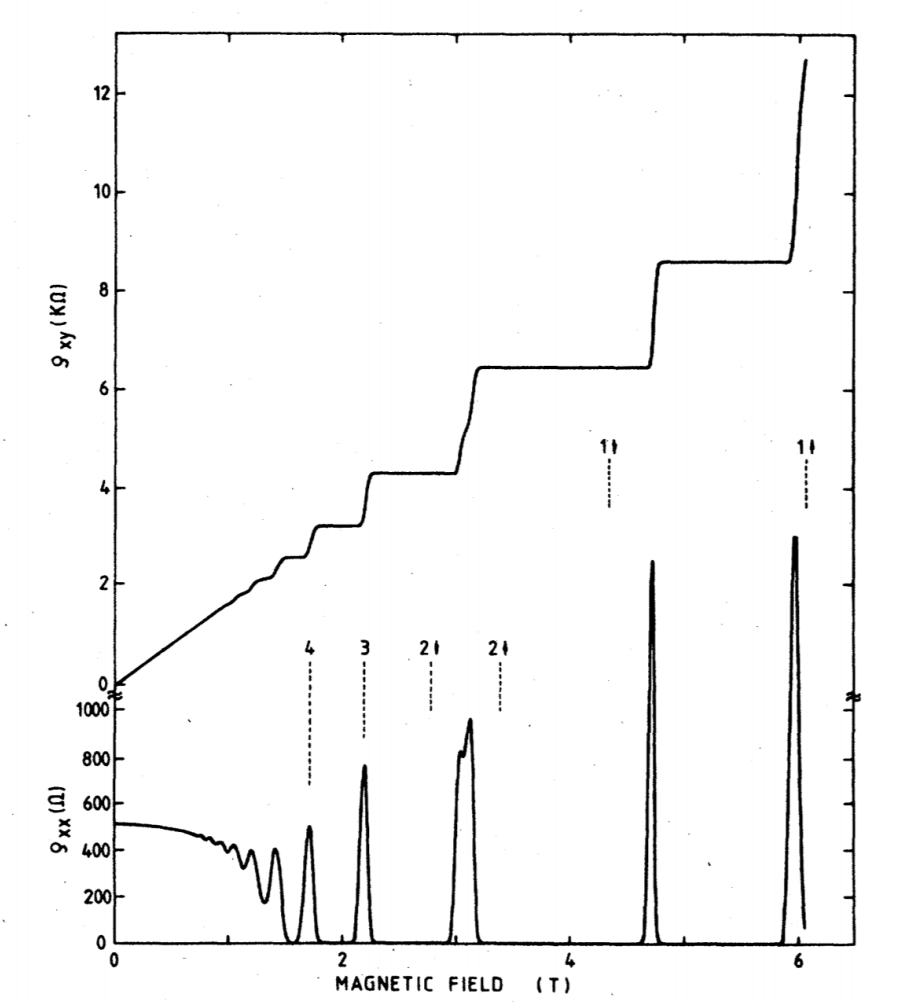

Figure 1.2: Experimental curves for the Hall resistance ρ_{xy} and the diagonal resistivity ρ_{xx}[41].

the gauge invariance of the Hamiltonian, a built-in fundamental symmetry. Consider imposing a periodical boundary condition in one direction on a 2DEG and effectively making the system into a ribbon-like structure (see Fig.(1.3)). The magnetic field is still perpendicular to the surface of the ribbon and there is another magnetic flux Φ threading through the area enclosed by the ribbon. Now imagine that we slowly crank up the magnetic flux ϕ, which induces an electric field circulating the ribbon and because of the Hall conductivity, there will be an electric flow from one open

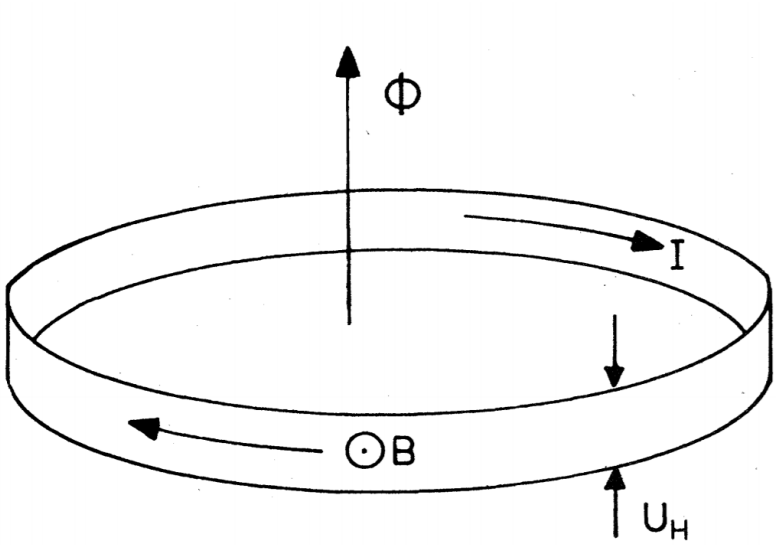

Figure 1.3: Configuration of a two-dimensional loop used for the thought-experiment proving robustness of quantized Hall conductivity[41].

boundary to the other. After we add exactly one more flux quantum

$$\Phi_0 = h/e, \tag{1.2}$$

the transferred charge $\sigma_{xy}\Phi_0$ should be an integer multiple of e and we arrive at the conclusion that σ_{xy} should be quantized as in Eq.(1.1).

Thouless *et al.*[39] gave the Kubo formula for the Hall conductivity within the framework of band theory and showed that the integer is mathematically the first Chern number of a U(1) bundle (associated with the arbitrary phase for the eigenstates) in the first Brillouin zone, which is topologically a torus.

The IQHE is the first example of phases that do not fit in Landau's symmetry breaking regime and opens the door to a whole new world of topological phases. In addition, it is not protected by any symmetry and can be called "intrinsically topological" compared to, *e.g.*, topological insulators which are protected by time-reversal symmetry[23].

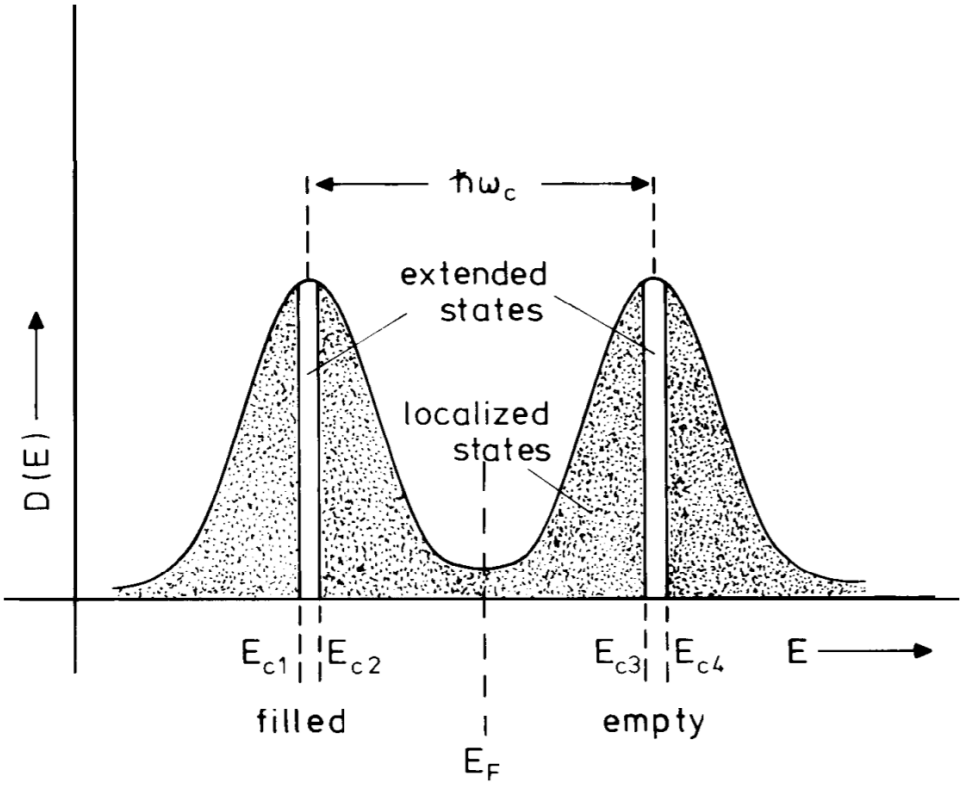

Figure 1.4: Schematic plot of the broadened density of states for the Landau levels due to disorders. Extended states sitting at the center are separated from localized states along the tails[41].

Interestingly, it's the presence of disorders that gives rise to the plateaus. The disorders broaden the Landau levels with extended states sitting at the center separated from localized states along the tails. See Fig.(1.4). A phase transition occurs when the Fermi energy sweeps through the extended states within a Landau level. In the range of the localized states transport property doesn't change, and therefore we see plateaus in the Hall conductivity curve. From a semiclassical point of view, the phase transition in the IQHE can be considered in a percolation picture. Model the disorders by a random potential that changes in a length scale much larger than the magnetic length $l_B = \sqrt{\hbar/eB}$ and the wave-packets of the electrons follow classical trajectories that are equipotential lines. In this picture localized states correspond to closed loops while extended states to open orbits. Increasing the Fermi is analo-

gous to filling a random landscape with water. When there is only a small amount of water, only the deepest valleys are filled. As the water level increases the small "puddles" will grow larger and start to merge. At a certain level a phase transition occurs where the boundaries of some large "lakes" percolate from one side of the system to the other. These boundaries are the extended states. Fig.(1.5) illustrates this process.

Another important feature of the IQHE is the presence of chiral edge currents. These chiral currents can only exist on the boundary of a 2D system, but not within an intrinsically 1D system. To understand why these edge modes emerge, we need the knowledge of Landau levels which is discussed in Sec.(1.3). Here we use classical mechanics to show that the chirality of the edge states is opposite to that of the Landau orbits. Fig.(1.6) shows an electron bouncing off the edge of a QHE droplet and the overall direction (clock-wise) is just opposite to that of the original Landau orbits (anti-clockwise).

1.2 FQHE

Although the fractional quantum Hall effect (FQHE) will not be the subject of this thesis, many important concepts that will be used in this thesis originally emerged from the study of the FQHE.

The FQHE was first discovered by Tsui *et al.* at 1/3 filling[40] and later at a filling with an even-denominator 5/2[44] (see Fig.(1.2)). The explanation provided in the experimental paper[40] was the formation of a Wigner solid or charge-density-wave state. It was not until Laughlin's enlightening paper[29] that people really started to understand the FQHE. By numerically studying a 3-electron system, Laughlin wrote

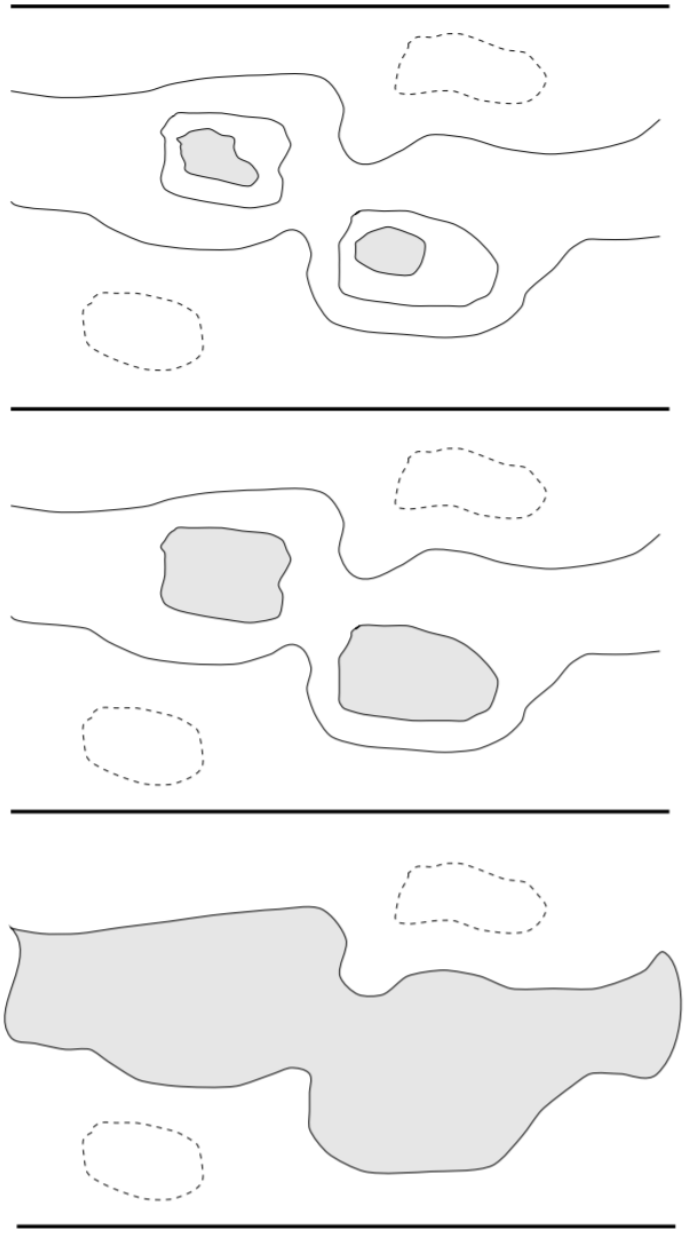

Figure 1.5: Contours of a random potential. Closed dashed lines are around "mountain peaks" and closed solid lines are around "valleys". Filled areas are regions below a certain level of the potential that increases from top to bottom. The bottom panel shows the extended boundary of the filled area that percolates from one side of the system to the other[12].

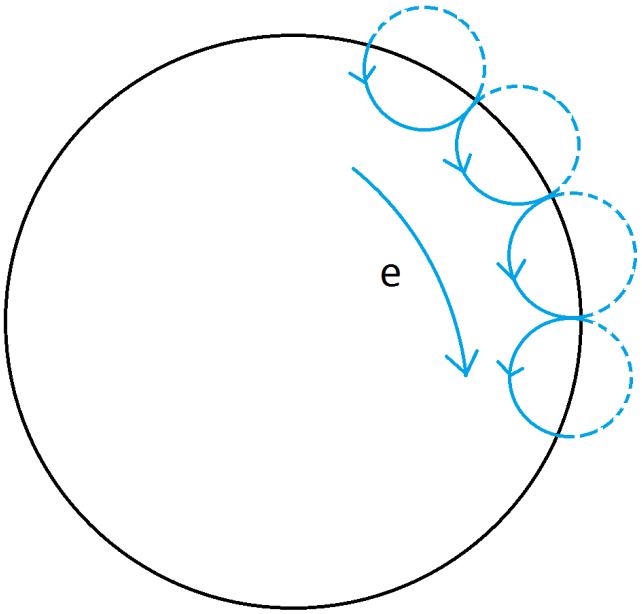

Figure 1.6: A schematic drawing showing anticlockwise Landau orbits (dashed lines are) and clockwise edge currents.

down his famous model wavefunction for the ground state on the Euclidean plane

$$\Psi_m = \prod_{i<j} (z_i - z_j)^m e^{-\frac{1}{2}\sum_i |z_i|^2}, \tag{1.3}$$

where $z = x+iy$ is the complex coordinate and m is an odd (even) integer for fermionic (bosonic) systems. He also constructed wavefunctions for charged excitations, namely quasiholes and quasiparticles. By realizing that

$$\ln |\Psi_m|^2 = \sum_{i<j} 2m \ln |z_i - z_j| - \sum_i |z_i|^2 \tag{1.4}$$

can be interpreted as the energy for a 2D Coulomb gas in a uniform neutralizing background, he argued that these excitations have a fractional charge $1/m$. Later their statistics were also calculated[2] and they were found to obey fractional statistics meaning that exchanging two such excitations results in a phase factor not necessarily

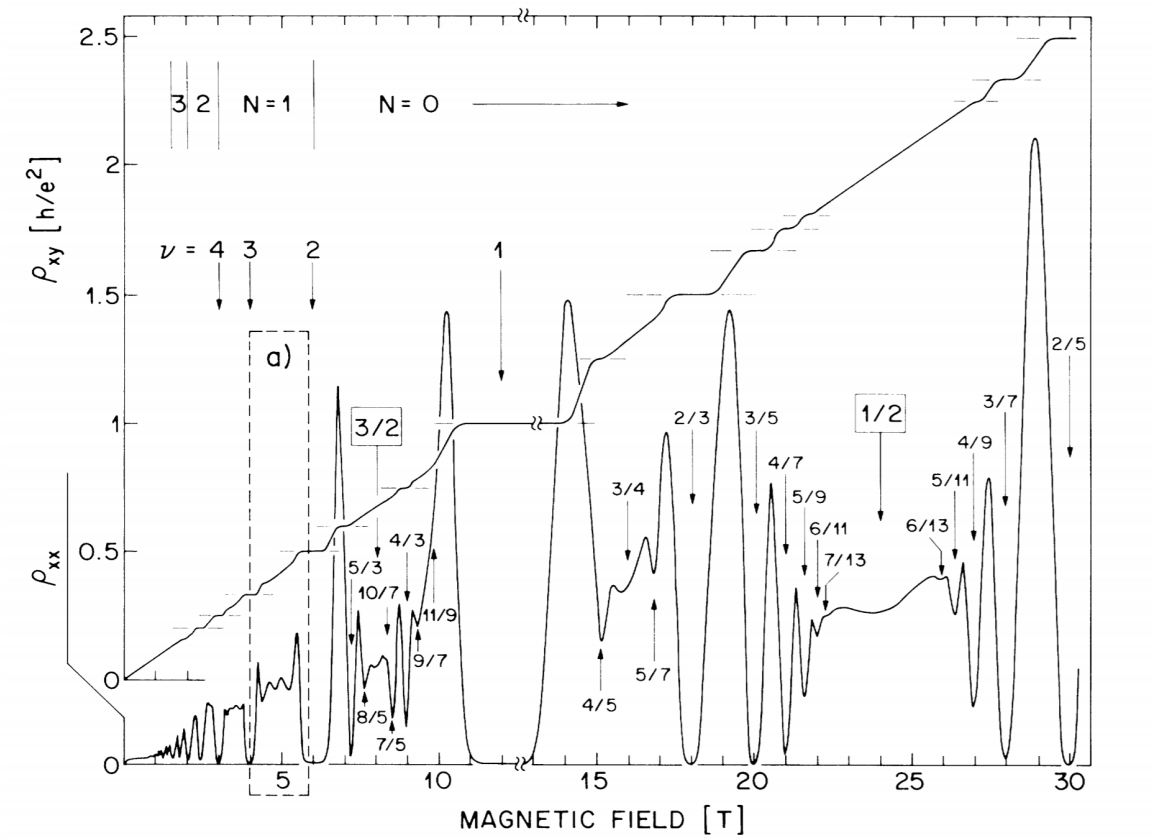

Figure 1.7: Integer and fractional quantum Hall plateaus for the Hall resistance ρ_{xy} and associated dips in the dissipative resistance ρ_{xx}[44].

equal to ± 1, as is the case for bosons and fermions. Despite all these achievements, the fact that the Laughlin wavefunction has a nearly perfect overlap with the true ground state under Coulomb interaction still seemed to be a magic at that time.

To understand the Laughlin wavefunction, Haldane[17] considered a quantum Hall system on the sphere, a compact manifold without boundary, and found that the Laughlin wavefunction is the exact eigenstate of a certain type of interaction called pseudopotentials. For example, on the plane a pseudopotential V_m is an operator projecting the relative angular momentum of two electron into $L_z = m$ sector. Ψ_m has the property that it is an exact zero state with $V_{m'} = 0$ for all $m' > m$, *i.e.*, in the Laughlin state no two electrons have a relative angular momentum $\leq m$. The Laughlin wave function works because it captures the behavior of the electrons when

they come close to each other. In other words, the FQHE is governed by the short-range part of the Coulomb interaction. In the same paper, Haldane also proposed a scheme for constructing a hierarchy of quantum Hall states at different fillings by proliferating the quasiholes or quasiparticles. For example, a quasiparticle in the 1/3 state can be viewed as a 2/5 droplet surrounded by all the other 1/3 droplets where a p/q droplet contains p electrons and q flux quanta. A similar construction was also proposed by Halperin[22]. The composite-fermion approach proposed by Jain is also an alternative to generate quantum Hall states[25].

The construction of neutral excitations came with the seminal paper by Girvin, Macdonald and Platzman[13]. The technique used there is closely analogous to Feynman's theory of superfluid helium. The neutral excitation is created by acting ρ_q, the density operator in the momentum space, on the ground state. The expression for the energy of the excitation is

$$E(q) = \frac{O(q^4 l^4)}{S(ql)}, \tag{1.5}$$

where $S(ql)$ is the static structure factor. This is called the magneto-roton mode and Fig.(1.2) shows the structure factor of 1/3 and 1/5 fillings. The peak of the structure factor gives rise to the minimum of the mode called the roton-minimum. At small q, the structure factors goes as q^4 so there is a finite gap at long wave length. The ripples at large q will become increasingly violent as the filling factor gets smaller signifying a possible phase transition to a periodic Wigner crystal[9].

Apart from the Laughlin series and the hierarchy series, there exist other types of quantum hall states. In their paper, Moore and Read[31] pointed out that the Laughlin wavefunctions were mathematical related to conformal blocks of 2D conformal field

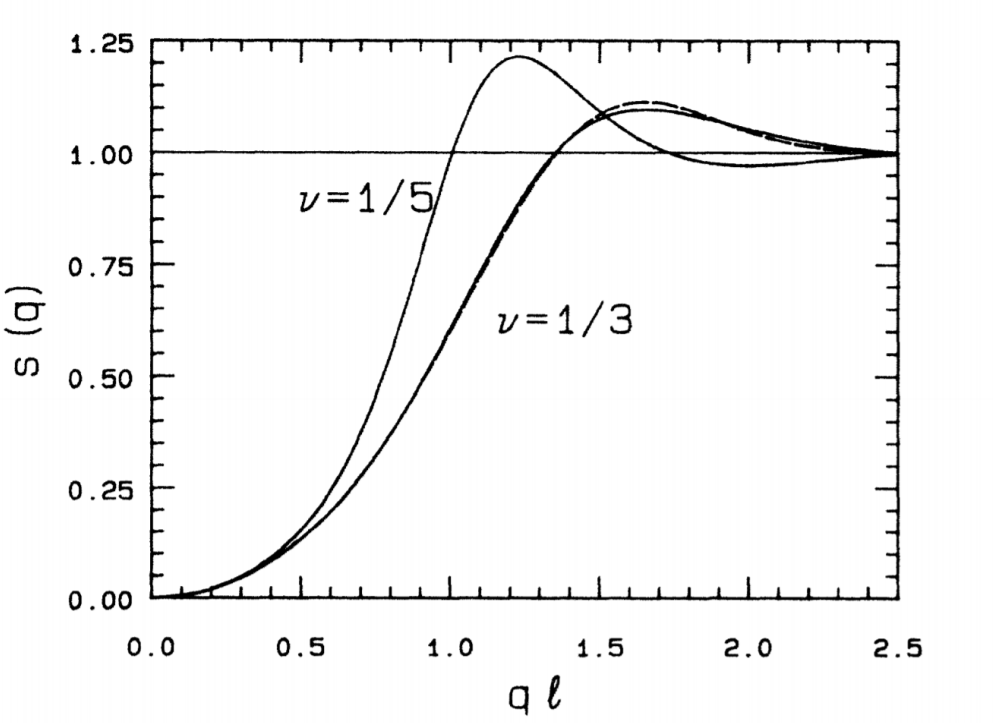

Figure 1.8: Static structure factor for Laughlin 1/3 state and 1/5 state. Solid line is modified-hypernetted-chain calculation. Dashed line is from fit to Monte Carlo data[13]. The peak of the structure factor gives rise to a roton-minimum at finite wave vector in the magneto-roton mode.

theory. They used this observation to construct a state in the form of

$$\Psi_{\rm MR} = \mathrm{Pfaff}\left(\frac{1}{z_i - z_j}\right)\prod_{i<j}(z_i - z_j)^2 e^{-\frac{1}{2}\sum_i |z_i|^2}, \tag{1.6}$$

where the Pfaffian is defined by

$$\mathrm{Pfaff}(M_{ij}) = \frac{1}{2^{N/2}(N/2)!}\sum_{\sigma\in S_N}\mathrm{sgn}\sigma\prod_{k=1}^{N/2} M_{\sigma(2k-1),\sigma(2k)} \tag{1.7}$$

with S_N being the permutation group. It is now called the Moore-Read state and is a candidate for the ground state of 5/2 filling (1/2 filling in the second Landau level). An amazing property of this state is that it possesses excitations that obey

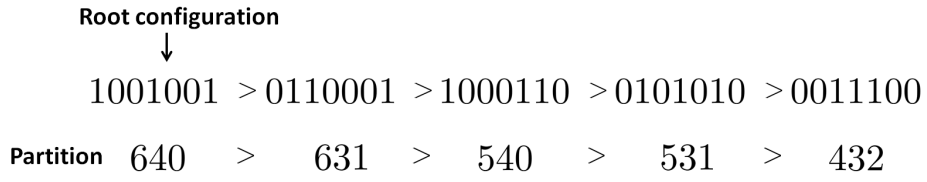

Figure 1.9: Order of slater determinants in the expansion of Laughlin 1/3 state with 3 electrons. The root configuration is 1001001, which is always the highest in order, and each Slater determinant corresponds to a partition (in this case of 10) by transcribing the position of each electron. The order of the partitions is determined by comparing the positions from left to right. The lower states can be obtained from squeezing two electrons closer to each other from higher states.

non-abelian braiding statistics[6]. They are building blocks of topological quantum computing[33]. The Read-Rezayi series are even more complicated states[37].

Notice that the model wavefunctions are all written in the first-quantized language. To transform them into the second-quantized language, *i.e.*, as an expansion in Fock basis (Slater determinants for fermionic systems) is not straightforward. Bernevig and Haldane[4] observed that the bosonic version of these model wavefunctions, for both the ground states and the excitations, were Jack polynomials. These polynomials are homogeneous and symmetric, constructed from a partition λ (called the "root configuration") and a parameter α. Each partition corresponds to a basis state in the Fock space and only those basis states that are lower in the order compared to the root configuration can appear in the expansion, where the order is defined by that of the partition. Fig.(1.9) shows an example. The coefficients of the expansion have a recursive relation that depends on α, which facilitates numerical generation of the wavefunctions. Model wavefunctions for neutral excitations constructed with Jack polynomials were proposed in Ref[45]. The interpretation of the neutral excitations is that (at least at large q) they are dipole moments formed by a quasiparticle and a quasihole. See Fig.(1.10).

The jack polynomials are still exact model wavefunctions while the matrix-product-state (MPS) representation[47] is a useful approximation of the model

$$
\begin{aligned}
&\dot{1}\dot{1}\mathring{0}\mathring{0}1001001001001\cdots L=2,\\
&\dot{1}\dot{1}\mathring{0}01\mathring{0}01001001001\cdots L=3,\\
&\dot{1}\dot{1}\mathring{0}0100\mathring{1}001001001\cdots L=4,\\
&\dot{1}\dot{1}\mathring{0}01001001\mathring{0}01001\cdots L=5,\\
&\dot{1}\dot{1}\mathring{0}0100100100\mathring{1}001\cdots L=6.\\
&\vdots
\end{aligned}
$$

Figure 1.10: Root configurations of model wavefunctions for neutral excitations for the Langhlin 1/3 system. The total angular momentum L is calculated with respect to the ground state (with root configuration $1001001\cdots1001$). Note the smallest L that can be created is 2. The black dots indicate the positions of quasiparticles while the white dots those of quasiholes. They are determined by counting the number of electrons in three consecutive orbitals. When L increases, the excitation can be roughly viewed as a pair of quasihole and quasiparticle that forms a dipole moment.

wavefunctions that further enables numerical calculations of various properties of the FQHE. This is closely related to the concept of entanglement spectrum that was introduced by Li and Haldane[30]. The universality within the entanglement spectrum of the model wavefunctions are closely related to the fact that they are identical to conformal blocks of a "bulk CFT" and that the cut that divides the system into two parts mimics the physical edge where an "edge CFT" describes the gapless edge excitations, which is investigated by Wen[42].

At first sight the models wavefunctions appear to be rigid in the sense that they contain no variational parameters. In a geometric description of the FQHE initiated by Haldane[19], a hidden degree of freedom called the guiding-center metric that defines the shape of the "correlation hole" around an electron can be tuned to minimize the Coulomb energy. This is numerically done in Ref[46]. Also the zero fluctuation of this metric gives rise to the gap at zero momentum. This metric is a dynamic quantity that has nothing to do with that of the underlying manifold. A metric of

free choice will be a critical concept in the generic theory for the IQHE presented in this thesis.

1.3 Continuous model

In this section we want to review the usual Galilean-invariant continuous model to illustrate some basic concepts and prepare the reader for later (more generic) discussions. Consider a 2DEG living on the infinite 2D Euclidean plane under a uniform magnetic field B. The dispersion is quadratic, *i.e.*, the Hamiltonian is in the form of

$$H = \frac{1}{2m}\left(p_x^2 + p_y^2\right), \quad p_{x,y} = -i\hbar\partial_{x,y} - eA_{x,y}. \tag{1.8}$$

We will use the so-called symmetry gauge $A_x = \frac{1}{2}By$ and $A_y = -\frac{1}{2}Bx$. The commutator of the momentum operators has a simple form,

$$[p_x, p_y] = i\hbar eB, \tag{1.9}$$

which is reminiscent of the canonical commutator $[x, p_x] = i\hbar$. Indeed, we can build ladder operators out of the momentum operators by

$$a = \frac{p_x + ip_y}{\sqrt{2\hbar eB}}, \quad a^\dagger = \frac{p_x - ip_y}{\sqrt{2\hbar eB}}, \tag{1.10}$$

so that $[a, a^\dagger] = 1$. The Hamiltonian is then

$$H = \hbar\omega_c(a^\dagger a + \tfrac{1}{2}), \quad \omega_c = eB/m. \tag{1.11}$$

The spectrum is thus equivalent to that of a harmonic oscillator

$$E_n = \hbar\omega_c(n + \tfrac{1}{2}), \tag{1.12}$$

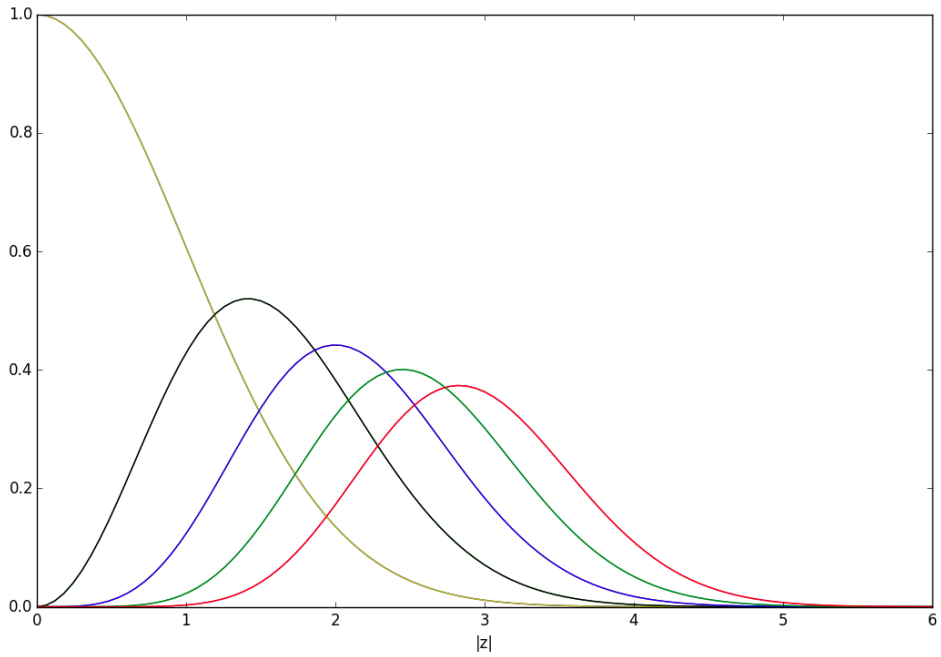

Figure 1.11: Lowest Landau level states $z^m e^{-\frac{1}{2}z^*z}/\sqrt{m!}$ with $m = 0, 2, 4, 6, 8$ plotted against $|z|$. Except the $m = 0$ state, they vanish at $|z| = 0$ and have a peak at $|z| = \sqrt{m}$.

except that now each level (called a Landau level) is macroscopically degenerate with a degeneracy equal to the number of flux quanta (at least for a flat geometry like the Euclidean plane). The eigenstates of the lowest Landau level satisfy $a|\Psi_0\rangle = 0$ and have a nice form using complex variable $z = (x + iy)/\sqrt{2}$

$$|\Psi_0\rangle = f(z)e^{-\frac{1}{2}z^*z}, \tag{1.13}$$

i.e., a holomorphic function times an exponential factor. An orthonormal basis can be chosen to be

$$|\Psi_{0,m}\rangle = \frac{z^m}{\sqrt{m!}}e^{-\frac{1}{2}z^*z}, \quad m = 0, 1, 2, \ldots \tag{1.14}$$

They are eigenstates of the angular momentum operator $L_z = x\partial_y - y\partial_x$ with eigen-

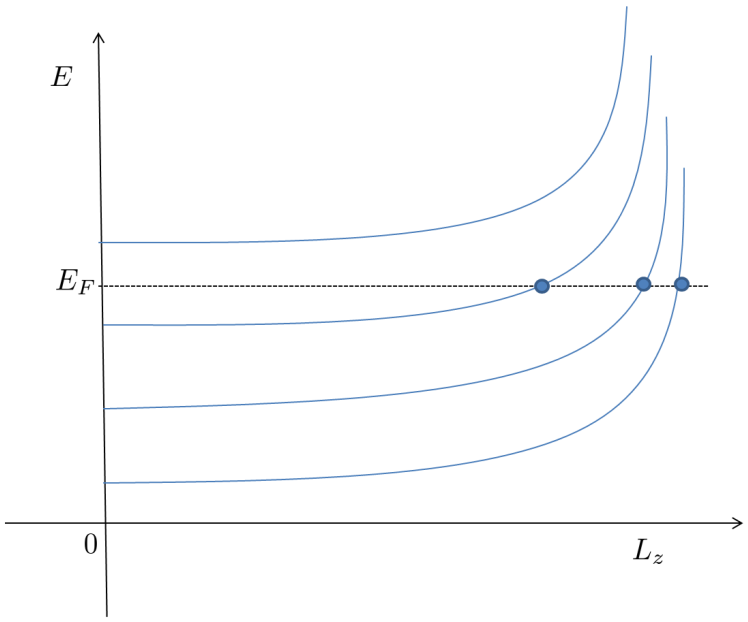

Figure 1.12: Landau levels under a rotationally invariant confining potential. The Fermi energy E_F is between the 2nd and the 3rd Landau levels and has three intersections with the lowest three Landau levels. Theses intersections correspond to three branches of gapless edge modes.

value m. Notice that the peak of $|\Psi_{0,m}|$ is at $|z| = \sqrt{m}$ (see Fig.(1.11)) so if we add a rotationally invariant confining potential that increases monotonically with $|z|$ then we will have a spectrum where (in each Landau level) energy increases with angular momentum index. See Fig. (1.12). Then if we set the Fermi energy just above the nth Landau level, it will have n intersections with the lowest n bands, creating n gapless edge modes.

We want to look at in particular $|\Psi_{0,0}\rangle = e^{-\frac{1}{2}z^*z}$, which is a coherent state centered at the origin. If we "raise" the state using $a^\dagger$ we will have a series of states

$$(a^\dagger)^k|\Psi_{0,0}\rangle = (z^*)^k e^{-\frac{1}{2}z^*z}. \tag{1.15}$$

These can be called coherent states in the kth Landau level. In the next chapter we will see that a coherent state (in any Landau level) will have a generic form

$$f(z^*)e^{-\frac{1}{2}z^*z} \tag{1.16}$$

in the absence of Galilean or rotational symmetry.

1.4 Galilean and rotational symmetries

In the previous section we modeled the IQHE using a quadratic Hamiltonian with Euclidean metric. That Hamiltonian has both Galilean and rotational symmetries. A general Galilean-invariant Hamiltonian is

$$H = \frac{1}{2}m^{ab}p_a p_b, \tag{1.17}$$

where m^{ab} is the inverse mass tensor inherited from the band structure. A general rotationally invariant Hamiltonian is

$$H = \sum_{k=1}^{K} c_k \left(g^{ab}p_a p_b\right)^k, \tag{1.18}$$

where the metric is the same for every term. A Hamiltonian in this form can still be exactly diagonalized using the same technique as in the Galilean invariant case. It's just that the energy levels are not evenly separated.

There has been recent interest in geometrical properties of the QHE[7, 8, 1, 15, 10, 11, 16, 38]. A typical field-theoretical model that is used in the literature is

$$S = \int d^2x dt \sqrt{g}\left[\frac{i}{2}\hbar\psi^\dagger\partial_0\psi - \frac{i}{2}\hbar(\partial_0\psi^\dagger)\psi + eA_0\psi^\dagger\psi - \frac{\hbar^2}{2m}g^{ij}(D_i\psi)^\dagger D_j\psi + \frac{g_s B}{4m}\psi^\dagger\psi\right], \tag{1.19}$$

which clearly has Galilean symmetry. The Newton-Cartan geometry proposed in Ref.[38] is also a generalization of the Galilean symmetry. However, these are not generic symmetries for electrons moving in a crystal background and can only be viewed as a lowest order expansion of the band structure around a band minimum. A simple toy model is certainly useful in revealing the basic properties of the QHE, especially the topological ones since they are, by nature, not related to the presence or absence of symmetries and a simple model offers an easy way to calculate them. However, for geometrical properties of the QHE the use of special symmetries might obscure fine structures in the system and thus can be potentially misleading. We would like to overcome this obstacle in understanding the IQHE.

1.5 Road map

The purpose of this thesis is to present a generic theory of the IQHE in the absence of Galilean or rotational symmetry. Preparatory material discussing the algebra of Landau orbits and guiding centers is provided in Chap.(2). There we also construct guiding-center coherent states that will be studied in detail later. After that we will achieve two goals. The first is to properly characterize the coherent state in each Landau level, which is done numerically in Chap.(3) for a quartic Hamiltonian. A topological quantity called the topological spin will be introduced there by investigating the root distribution of the antiholomorphic part of the coherent states. The second goal is to clarify distinct geometrical properties for the IQHE. In Chap.(4) a generic formula for the Hall viscosity, response to a non-uniform flow velocity field, will be derived and compared to previous results in the literature. In Chap.(5) we will calculate generic electromagnetic responses and differentiate between universal terms that are diagonal in the Landau levels and non-universal terms that depend on inter-Landau-level mixing. Conclusions can be found in Chap.(6).

Chapter 2

A generic approach

Since we want to forfeit Galilean and rotational symmetries, we need a generic approach to address the IQHE problem. We will first introduce the algebra of Landau orbits and guiding centers, two independent degrees of freedom. They both possess a metric of free choice. Then we will define the guiding-center coherent states by providing a natural choice for the guiding-center metric. After presenting a generic form of the single-particle Hamiltonian we will look closely at the quartic case, which will be studied in detail numerically in the next chapter.

2.1 The algebra of Landau orbits and guiding centers

As mentioned in Sec.(1.3), the 2D dynamic momentum operator is defined as

$$p_a = -i\hbar\partial_a - eA_a(\boldsymbol{x}), \tag{2.1}$$

with the commutator being

$$[p_a, p_b] = i\hbar e\epsilon_{ab} B(\boldsymbol{x}). \tag{2.2}$$

We have used the fact that

$$\partial_a A_b - \partial_b A_a = B(\boldsymbol{x})\epsilon_{ab} \tag{2.3}$$

which is true regardless of gauge choice. We will focus on the case of a uniform magnetic field $B(\boldsymbol{x}) = B$ and leave perturbations to Chap.(5) where we discuss electromagnetic response functions. Now decompose the electron coordinate as follows,

$$x^a = R^a + \tilde{R}^a, \tag{2.4}$$

$$\tilde{R}^a \equiv (eB)^{-1}\epsilon^{ab} p_b, \tag{2.5}$$

where R^a is the "guiding-center" coordinate and $\tilde{R}^a$ is the Landau-orbit coordinate. The physical interpretation of this decomposition is that the guiding-center coordinate describes the position of the center of the orbit with respect to the origin while the Landau-level coordinate describes the relative position of the electron to the orbit center, as shown in Fig.(2.1). An amazing property of this decomposition is that the two parts are independent degrees of freedom, i.e.,

$$[R^a, \tilde{R}^b] = 0. \tag{2.6}$$

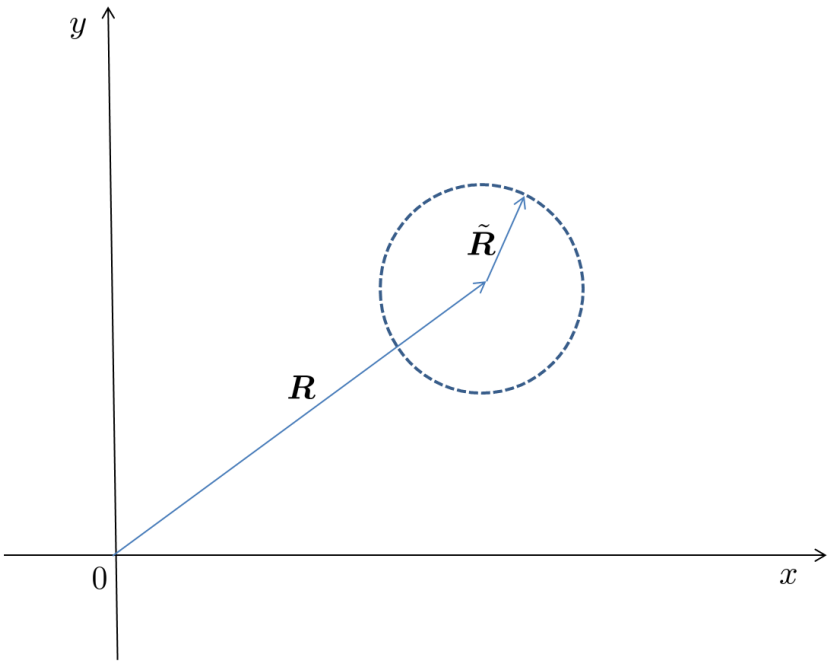

Figure 2.1: Landau-orbit coordinate $\tilde{\boldsymbol{R}}$ and guiding-center coordinate $\boldsymbol{R}$.

However these coordinates are not classical quantities, *i.e.*, they have non-trivial commutators,

$$[R^a, R^b] = -i\hbar(eB)^{-1}\epsilon^{ab}, \tag{2.7}$$

$$[\tilde{R}^a, \tilde{R}^b] = i\hbar(eB)^{-1}\epsilon^{ab}, \tag{2.8}$$

and thus can not be diagonalized simultaneously, unlike the usual coordinate operators in the Schrödinger picture where $\hat{\boldsymbol{x}}|\boldsymbol{x}\rangle = \boldsymbol{x}|\boldsymbol{x}\rangle$. The best we can do is to construct a coherent state that is physically a fuzzy object saturating Heisenberg's uncertainty principle, which is detailed in the next section. Also notice that the commutators have opposite signs, which is another manifestation of the opposite chiralities of Landau orbits and edge states (guiding-center flow) mentioned in Sec.(1.1).

We can define *two* sets of harmonic-oscillator operators for Landau-orbit and guiding-center degrees of freedom respectively,

$$a = \sqrt{\frac{eB}{2\hbar}}\tilde{e}_a \tilde{R}^a, \qquad b = \sqrt{\frac{eB}{2\hbar}}\bar{e}_a R^a, \tag{2.9}$$

$$a^\dagger = \sqrt{\frac{eB}{2\hbar}}\tilde{e}^*_a \tilde{R}^a, \qquad b^\dagger = \sqrt{\frac{eB}{2\hbar}}\bar{e}^*_a R^a, \tag{2.10}$$

where the e_a, called (complex 2D) frame fields, satisfy

$$\epsilon^{ab}\tilde{e}^*_a\tilde{e}_b = \epsilon^{ab}\bar{e}^*_a\bar{e}_b = i, \tag{2.11}$$

so that the harmonic-oscillator operators have the expected commutation relations $[a, a^\dagger] = [b, b^\dagger] = 1, [a, b] = [a, b^\dagger] = 0$. This fixes the antisymmetric part of $e_a e_b$ and we can define a metric from the symmetric part for both Landau-orbit and guiding-center sectors,

$$\tilde{g}_{ab} = \tilde{e}^*_a\tilde{e}_b + \tilde{e}^*_b\tilde{e}_a, \quad \bar{g}_{ab} = \bar{e}^*_a\bar{e}_b + \bar{e}^*_b\bar{e}_a. \tag{2.12}$$

These metrics are *unimodular* meaning that the determinant

$$\det g = \tfrac{1}{2}\epsilon^{ac}\epsilon^{bd}g_{ab}g_{cd} \tag{2.13}$$

is 1. The inverse metrics are then

$$\tilde{g}^{ab} = \epsilon^{ac}\epsilon^{bd}\tilde{g}_{cd}, \quad \bar{g}^{ab} = \epsilon^{ac}\epsilon^{bd}\bar{g}_{cd}. \tag{2.14}$$

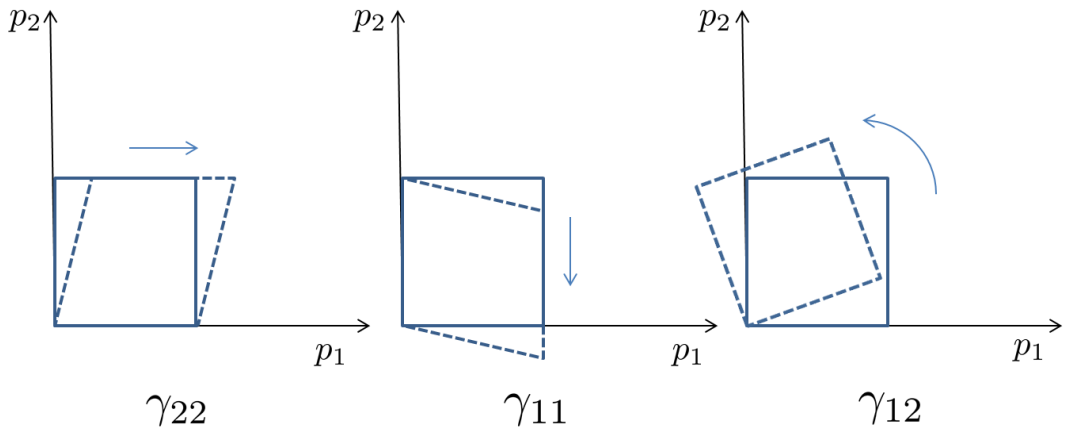

Figure 2.2: Schematic drawing of the effect of three area-preserving generators γ_{22}, γ_{11}, and γ_{12}. γ_{22} and γ_{11} translate one of the two momentum operators while γ_{12} is a rotation.

Up until now we have not specified the frame fields or the metrics. In fact different choices are related by Bogliubov transformations

$$\begin{pmatrix} a' \\ a'^{\dagger} \end{pmatrix} = \begin{pmatrix} e^{i\phi_1}\cosh\theta & e^{i\phi_2}\sinh\theta \\ e^{-i\phi_2}\sinh\theta & e^{-i\phi_1}\cosh\theta \end{pmatrix} \begin{pmatrix} a \\ a^{\dagger} \end{pmatrix} \tag{2.15}$$

parametrized by three parameters ϕ_1, ϕ_2 and θ. This can also be viewed from the perspective of area-preserving deformations of the momentum-space

$$p_a \to U(\beta) p_a U(\beta)^{-1}. \tag{2.16}$$

The unitary operator $U(\beta)$ is defined as

$$U(\beta) = \exp(i\pi\beta^{ab}\gamma_{ab}), \tag{2.17}$$

$$\gamma_{ab} = (4\hbar eB)^{-1}\{p_a, p_b\}, \tag{2.18}$$

where β_{ab} is a real symmetric matrix. The action of the generators can be understood by calculating their commutators with the momentum operators

$$[p_a, \gamma_{bc}] = \tfrac{1}{2} i(\epsilon_{ab} p_c + \epsilon_{ac} p_b). \tag{2.19}$$

We can see that γ_{11} leaves p_1 invariant while translates p_2 in the direction of p_1. γ_{22} acts in a similar way and γ_{12} corresponds to a rotation, as illustrated in Fig. (2.2). These generators obey a Lie-algebra

$$[\gamma_{ab}, \gamma_{cd}] = \tfrac{1}{2} i(\epsilon_{ac}\gamma_{bd} + \epsilon_{bc}\gamma_{ad} + \epsilon_{ad}\gamma_{bc} + \epsilon_{bd}\gamma_{ac}) \tag{2.20}$$

that will be useful in deriving the Hall viscosity in Sec. (4.3).

If the system under study has rotational symmetry, it's natural to identify the two metrics, then the z-component of the angular momentum operator written as

$$L_z = b^\dagger b - a^\dagger a = b^\dagger b + \tfrac{1}{2} - (a^\dagger a + \tfrac{1}{2}) \tag{2.21}$$

is a good quantum number. We have a finer structure of the spectrum now by realizing that in nth Landau level the smallest L_z is $-n$, as illustrated in Fig.(2.3).

The differentiation between two independent and fundamentally arbitrary metrics is critical in our generic description for the IQHE without Galilean or rotational symmetry. In the next section we will introduce what we think is the most natural choice for the guiding-center metric in the process of defining guiding-center coherent states.

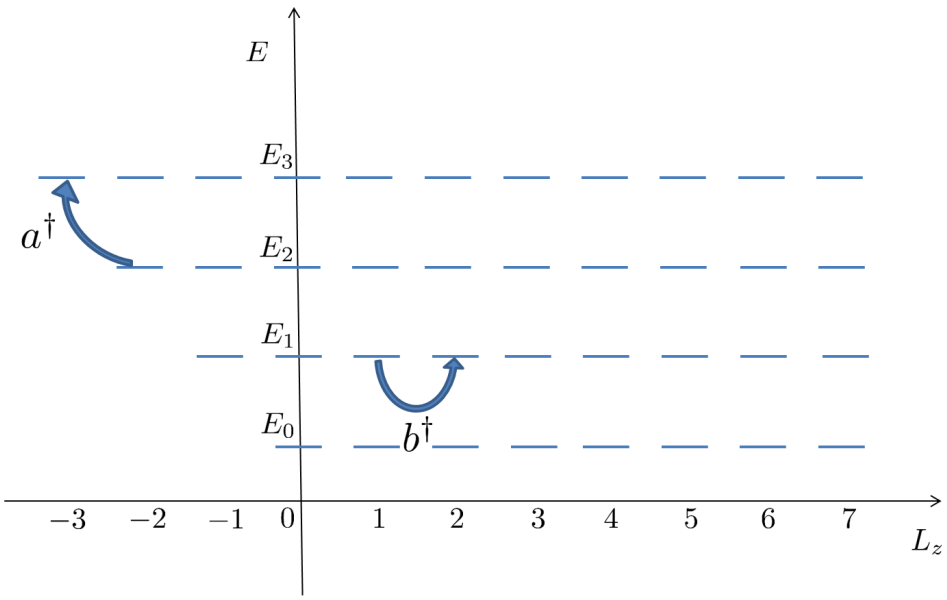

Figure 2.3: Sketch of the single-particle spectrum for a rotationally invariant quantum Hall system. The z-component of the angular momentum $L_z = b^\dagger b - a^\dagger a$ is a good quantum number and the lowest L_z for the nth Landau level is $-n$. $a^\dagger$ raises a state to the next Landau level and lowers L_z by 1 while $b^\dagger$ raises a state to the next L_z eigenstate within the same Landau level.

2.2 Guiding-center coherent states

We said at the end of the introductory chapter that we wanted to characterize the eigenstates at the absence of rotational symmetry. Since a Landau level is macroscopically degenerate (this is due to the existence of two independent sets of algebra), we need to look at a specific state in each Landau level and a coherent state would be a good candidate. Then comes the problem of how to construct these coherent states.

We inherit the spirit of a usual coherent state, which is the closest quantum mechanical state to the classical state, and define here a guiding-center coherent state with a fixed guiding center

$$\langle \Psi_n(\bar{\boldsymbol{x}}, \bar{g}) | \boldsymbol{R} | \langle \Psi_n(\bar{\boldsymbol{x}}, \bar{g}) \rangle = \bar{\boldsymbol{x}} \tag{2.22}$$

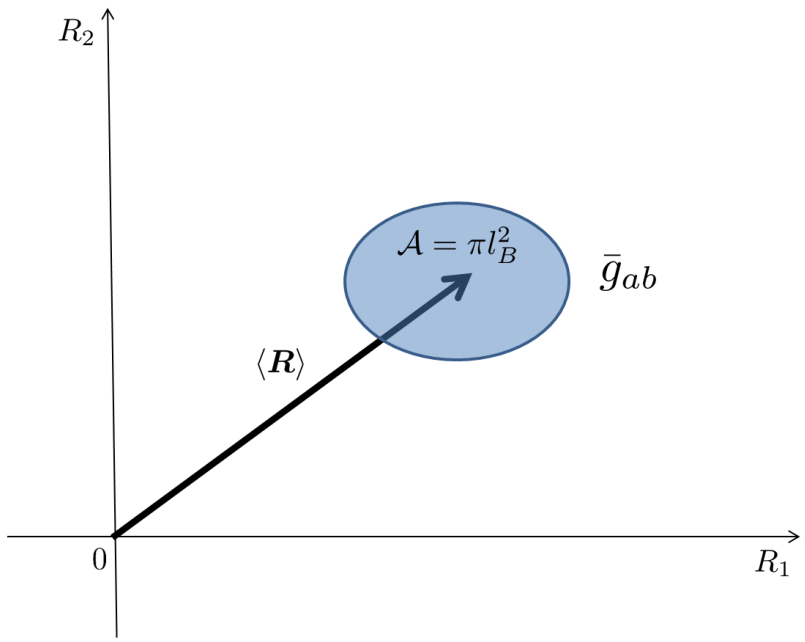

Figure 2.4: A coherent state on the guiding-center plane (analogous to the phase space of a harmonic oscillator). The coordinates of the center of the coherent state indicate the expectation values of the guiding-center operators. The shape of the coherent state is determined by the guiding-center metric and the area of the fuzzy region is πl_B^2. The combination of this uncertainty with that of the Landau orbits, also πl_B^2, gives the area per flux quantum $2\pi l_B^2$.

that satisfies

$$\bar{g}_{ab}(\langle\Psi|R^a R^b|\Psi\rangle - \langle\Psi|R^a|\Psi\rangle\langle\Psi|R^b|\Psi\rangle) = \frac{\hbar}{eB} \equiv l_B^2, \tag{2.23}$$

i.e., the guiding-center part saturates Heisenberg's uncertainty principle as an equality. Fig.(2.4) illustrates such a coherent state on the guiding-center plane (similar to the phase space of a harmonic oscillator). Without loss of generality, we will only consider the case $\bar{\boldsymbol{x}} = 0$, a coherent state centered at the origin. Notice that the coherent state explicitly depends on the guiding-center metric and different choices of the metric correspond to physically distinct states. It turns out that there is a "natural" choice for each Landau level that is proportional to the expectation value

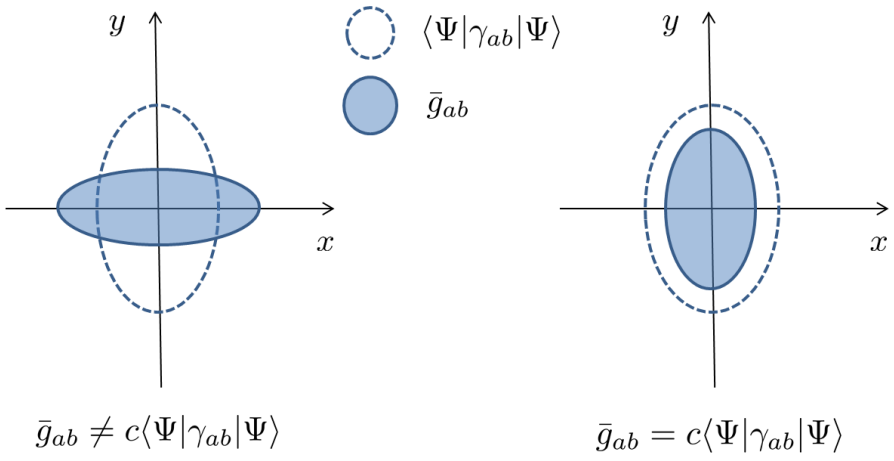

Figure 2.5: Shape of Landau orbits (dashed) determined by the expectation values of the area-preserving transformation generators γ_{ab} and that of guiding centers determined by $\bar{g}_{ab}$ (solid). In the right plot the two shapes are congruent, which is the case for the guiding-center coherent states that will be of interest to us.

of the γ_{ab} operators in that level

$$\bar{g}_{ab} \propto \langle\Psi_n|\gamma_{ab}|\Psi_n\rangle. \tag{2.24}$$

This natural metric, denoted g^n_{ab}, is generically different for each Landau level at the absence of rotational symmetry as it characterizes the shape of the orbits in each level. Using it to define the guiding-center coherent states, we are intentionally identifying the shape of guiding centers and that of Landau orbits. See Fig. (2.5). We will provide a more convincing justification of this choice in the next chapter where we investigate numerical solutions for the coherent states. The same metric is also proportional to the "2D Hall viscosity tensor" that will be introduced in Chap. (4).

We can obtain a more explicit expression for the coherent states by defining a complex structure on the 2D Euclidean plane

$$z = \bar{e}_a x^a/(\sqrt{2}l_B), \tag{2.25}$$

and picking a "symmetric" gauge for the vector potential

$$A_a(\boldsymbol{x}) = \frac{1}{\sqrt{2}} i(z^* \bar{e}_a - z\bar{e}_a^*). \tag{2.26}$$

This gauge is more generic in the sense that it contains an arbitrary field $\bar{e}_a$ that goes hand in hand with the guiding-center metric $\bar{g}_{ab}$. Notice that when $\bar{\boldsymbol{e}} = (1, i)/\sqrt{2}$ we go back to the usual symmetric gauge introduced in Sec.(1.3). Now the guiding-center harmonic-oscillator operators have explicit expressions

$$b = \tfrac{1}{2} z^* + \partial_z, \quad b^\dagger = \tfrac{1}{2} z - \partial_{z^*}. \tag{2.27}$$

We use an alternative definition of a coherent state (centered at the origin)

$$b|\Psi_n\rangle = 0 \tag{2.28}$$

to obtain a generic form

$$\Psi_n(z, z^*) = f_n(z^*) e^{-\frac{1}{2} z^* z}, \tag{2.29}$$

where the metric dependence is implicit in the definition of z. We see that it is an anti-holomorphic function times an exponential part. This is quite reminiscent (but should be differentiated from) the well-known property of lowest Landau level wavefunctions (a holomorphic function times an exponential factor) mentioned in Sec. (1.3) .

2.3 A generic Hamiltonian

In Sec.(1.4) we clarified what we meant by Galilean and rotational symmetries for a single-particle Hamiltonian. Now we will introduce a generic Hamiltonian in terms of the momentum operators

$$H(\boldsymbol{p}) = \sum_{k=1}^{n} \frac{1}{(2k)!} H^{a_1 a_2 \ldots a_{2k}} p_{a_1} p_{a_2} \ldots p_{a_{2k}}, \tag{2.30}$$

where the coefficients $H^{a_1 a_2 \ldots a_{2k}}$ are fully symmetric in the indices. The Hamiltonian contains only even order terms and has inversion symmetry

$$H(\boldsymbol{p}) = H(-\boldsymbol{p}). \tag{2.31}$$

For an arbitrary function $f(\boldsymbol{p})$ to be well-defined when the two variables p_a are non-commuting, it should be an *entire* function meaning that for any c-number $\boldsymbol{p}_0$, $f(\boldsymbol{p}_0 + (\boldsymbol{p} - \boldsymbol{p}_0))$ expanded in powers of $\delta\boldsymbol{p} = \boldsymbol{p} - \boldsymbol{p}_0$

$$f(\boldsymbol{p}) = \sum_{n=0}^{\infty} f^{a_1 a_2 \ldots a_n}(\boldsymbol{p}_0)\{\delta p_{a_1}, \ldots, \delta p_{a_n}\}, \tag{2.32}$$

where $\{\ldots\}$ is a symmetrized product, is absolutely convergent. The Hamiltonian defined here is a polynomial in p_a so the condition is always satisfied. For it to be bounded below, the coefficient for the highest term needs to be positive semi-definite, i.e.,

$$A^{a_1 a_2 \ldots a_{2n}} p_{a_1} p_{a_2} \ldots p_{a_{2n}} \geq 0 \tag{2.33}$$

for all $\boldsymbol{p} \neq \boldsymbol{0}$. But we will impose a stricter condition here that for all $\boldsymbol{p} \neq \boldsymbol{0}$, $\varepsilon(\lambda\boldsymbol{p})$, the classical version of $H(\lambda\boldsymbol{p})$ by treating $\boldsymbol{p}$ as a c-number, is strictly monotonically increasing for $0 \leq \lambda < \infty$ and unbounded as $\lambda \to \infty$. This constraint guarantees that

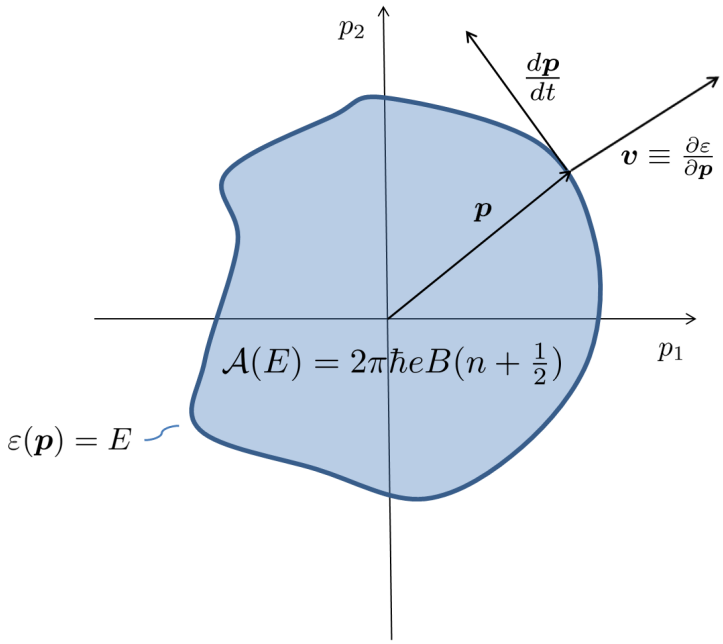

Figure 2.6: Semiclassical quantization of Landau orbits. The semiclassical orbits are closed equipotential lines of the dispersion relation $\varepsilon(\boldsymbol{p})$ and the area enclosed by the orbit is quantized according to $\mathcal{A}(E_n) = 2\pi\hbar eB(n + \frac{1}{2})$.

any curve determined by the equation $\varepsilon(\boldsymbol{p}) = E > \varepsilon(\boldsymbol{0})$ is topologically equivalent to a circle S_1 that encloses the origin. The curves are actually classical orbits as the equations of motion are

$$\frac{dx^a}{dt} = \frac{\partial \varepsilon}{\partial p_a} \equiv v^a, \quad \frac{dp_a}{dt} = eB\epsilon_{ab}v^b, \tag{2.34}$$

so the change in $\boldsymbol{p}$ is always perpendicular to the gradient field $\boldsymbol{v}$. Bohr-Sommerfeld quantization can be applied so the area enclosed by these curves are quantized as

$$\mathcal{A}(E_n) = 2\pi\hbar eB(n + \tfrac{1}{2}), \tag{2.35}$$

and the corresponding E_n are the Landau level energies. See Fig. (2.6). This will be revisited for numerical solutions in the next chapter.

To diagonalize the Hamiltonian, we still need to transform the momentum operators to harmonic-oscillator operators a and $a^\dagger$. When rotational symmetry is absent, there is no "best" choice of the metric $\tilde{g}_{ab}$ that puts the Hamiltonian in a readily diagonalizable form. However, since we introduced a natural metric for the guiding-center coherent states defined in the last section, using the same metric for $\tilde{g}_{ab}$ will make a and $a^\dagger$ expressible with the same complex structure z as

$$a = \tfrac{1}{2}z + \partial_{z^*}, \quad a^\dagger = \tfrac{1}{2}z^* - \partial_z, \tag{2.36}$$

and a coherent state that is also an eigenstate of $a^\dagger a$ with eigenvalue n is

$$\Psi_n^0 = \frac{(z^*)^n}{\sqrt{n!}} e^{-\frac{1}{2}z^* z}. \tag{2.37}$$

Thus a coherent state in the nth Landau level Ψ_n as an expansion in the Ψ_n^0, a result of diagonalizing the Hamiltonian, can be readily expressed as a Taylor expansion in terms of z^*, i.e.,

$$\Psi_n = \sum_{k=0}^{\infty} c_k \Psi_k^0 = \sum_{k=0}^{\infty} c_k \frac{(z^*)^k}{\sqrt{k!}} e^{-\frac{1}{2}z^* z}, \tag{2.38}$$

which is a clean form for further investigation. In the next chapter we will employ numerical methods to diagonalize the Hamiltonian and obtain the expansion with a cutoff on the number of available Ψ_n^0.

2.4 The quartic case

From now on we will focus on the simplest non-trivial case where the Hamiltonian only has quadratic and quartic terms, *i.e.*,

$$H = A_1^{ab} p_a p_b + A_2^{abcd} p_a p_b p_c p_d. \tag{2.39}$$

Let's look at the quartic term. If we treat the components of $\boldsymbol{p}$ as classical variables, $A_2^{abcd} p_a p_b p_c p_d$ is then a homogeneous polynomial of degree four and can be transformed into a univariate polynomial of p_1/p_2. This polynomial can have: I) two pairs of complex conjugate roots, II) one pair of complex conjugate roots and a real root of multiplicity 2, III) two real roots each of multiplicity 2, and IV) one real root of multiplicity 4. The existence of a pair of complex conjugate roots means the corresponding quadratic form is positive-definite and therefore the coefficient matrix can be interpreted as a metric. Based on this consideration, those four cases correspond to four different classes (labeled by Roman numerals) of the quartic term

$$A_{2,\mathrm{I}}^{ab,cd} = g_1^{ab} g_2^{cd} + g_2^{ab} g_1^{cd}, \quad \tfrac{1}{2}(g_1^{ab} + g_2^{ab}) = c g_0^{ab}, \tag{2.40}$$

$$A_{2,\mathrm{II}}^{ab,cd} = g_1^{ab} u_1^c u_1^d + u_1^a u_1^b g_1^{cd}, \tag{2.41}$$

$$A_{2,\mathrm{III}}^{ab,cd} = u_1^a u_1^b u_2^c u_2^d + u_2^a u_2^b u_1^c u_1^d, \;\; u_1^a u_1^b + u_2^a u_2^b = \lambda g_0^{ab}, \tag{2.42}$$

$$A_{2,\mathrm{IV}}^{ab,cd} = u_1^a u_1^b u_1^c u_1^d, \tag{2.43}$$

where $\lambda > 0$, and $c \geq 1$. The contour plots in the momentum space for a typical member in each class is plotted in Fig.(2.7). It can be seen that only class I has closed contours so it will be our main focus. There are two metrics g_1^{ab} and g_2^{ab} in the definition. After a $SL(2, R)$ transformation, as illustrated in Fig.(2.8), we can put

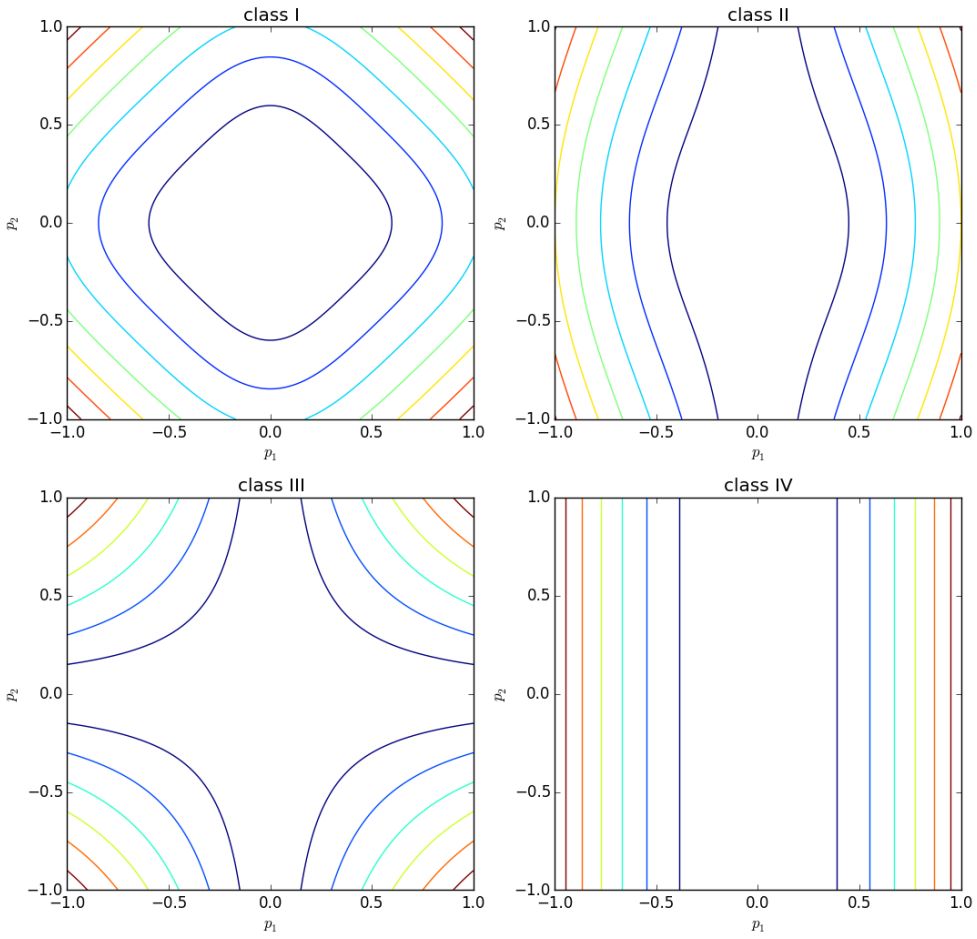

Figure 2.7: Contour plots in the momentum space of a typical member in each class of the quartic term. The quartic terms are I) $\{5p_1^2 + p_2^2, p_1^2 + 5p_2^2\}$, II) $\{p_1^2, p_1^2 + p_2^2\}$, III) $\{p_1^2, p_2^2\}$ and IV) p_1^4. Notice that only the contours for class I are closed.

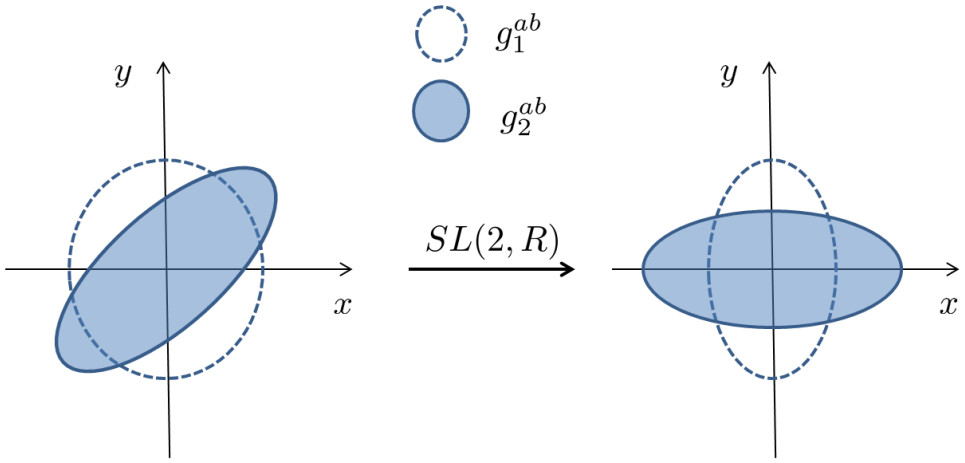

Figure 2.8: Sketch of creating C_4 symmetry under a $SL(2,R)$ transformation. Starting from $g_1^{ab} = \delta^{ab}$ (which can always be achieved under a certain basis), a rotation can put g_2^{ab} into a diagonal form. Then a scaling of one axis can put the two metrics into the final configuration where g_1^{ab} and g_2^{ab} are both diagonal and related by a 90 degree rotation.

these two metrics in the form

$$g_1^{ab} = \begin{pmatrix} d_1 & 0 \\ 0 & d_2 \end{pmatrix}, \quad g_2^{ab} = \begin{pmatrix} d_2 & 0 \\ 0 & d_1 \end{pmatrix}. \tag{2.44}$$

This is indeed the case for the example provided in Fig.(2.7). The quartic term is then

$$H = E_0 \left((\gamma_{11} + \gamma_{22})^2 + (c-1)\{\gamma_{11}, \gamma_{22}\} \right). \tag{2.45}$$

This form has an explicit C_4 symmetry under $(p_1, p_2) \to (-p_2, p_1)$ or $\gamma_{11} \leftrightarrow \gamma_{22}$. However we should remark that this C_4 symmetry is only possessed by a pure quartic term and has no generic significance.

Chapter 3

Numerics

In the previous chapter we introduced a generic form of the single-particle Hamiltonian and looked closely at the quartic case. Unfortunately we were not able to diagonalize the Hamiltonian analytically, so in this chapter we will employ numerical methods. By imposing a cutoff on the number of available basis states we transform the problem into matrix diagonalization. After we obtain the eigenstates, which are in the form of a polynomial in z^* times a exponential factor, we will look at the root distribution of that polynomial and define a "topological spin" $s_n = n + \frac{1}{2}$ where n is the number of the central roots separated from the outer roots by the semiclassical orbit. Its connection to the "shift" will be explained. At the end of this chapter we will briefly talk about Nevanlinna theory that studies the zero distribution and growth rate for solutions of complex differential equations.

3.1 Algorithm

The major steps of the algorithm are shown in Fig.(3.1). In Eq.(2.24) we have specified the guiding-center metric for the coherent states to be the expectation values of γ_{ab}. However, before we diagonalize the Hamiltonian and obtain the eigenstates, we don't have that metric at hand. Nonetheless, diagonalization only requires specifying the

Landau-orbit metric and the choice doesn't affect the results (at least when there is no cutoff). Therefore as a first step, we pick the Euclidean metric δ_{ab} to define Landau-orbit harmonic-oscillator operators a and $a^\dagger$. After calculating the expectation values of γ_{ab} in a certain Landau level indexed by n, we re-define a and $a^\dagger$ using that natural metric g^n_{ab} and re-diagonalize the Hamiltonian under the new basis (eigenstates of $a^\dagger a$). To obtain the frame fields, use

$$\tilde{e}_a = g_{ab}\tilde{e}^b = i\epsilon_{ab}\tilde{e}^b, \tag{3.1}$$

or in matrix form (letting $\tilde{e}^a \propto (1, \alpha)$)

$$\begin{pmatrix} g_{11} & g_{12} \\ g_{21} & g_{22} \end{pmatrix} \begin{pmatrix} 1 \\ \alpha \end{pmatrix} = \begin{pmatrix} 0 & i \\ -i & 0 \end{pmatrix} \begin{pmatrix} 1 \\ \alpha \end{pmatrix}. \tag{3.2}$$

We have

$$\tilde{e}^a = \sqrt{\frac{g_{22}}{2}} \left(1, \frac{-g_{12} - i}{g_{22}}\right), \tag{3.3}$$

and $a = \tilde{e}^a p_a / \sqrt{\hbar e B}$. If we define

$$p^E_1 = (a + a^\dagger)/\sqrt{2}, \quad p^E_2 = -i(a - a^\dagger)/\sqrt{2}, \tag{3.4}$$

then the expectation value of $\{p^E_a, p^E_b\}$ in the nth eigenstate should be the Euclidean metric δ_{ab}. This can be checked to make sure that the algorithm is working properly.

We then pick the nth eigenstate, whose natural metric now defines both $a^\dagger$ and $b^\dagger$. The eigenstate has a representation (with a cutoff on the available orbitals)

$$\Psi_n = \sum_{k=0}^{N} c_k \frac{(z^*)^k}{\sqrt{k!}} e^{-\frac{1}{2}z^* z}, \tag{3.5}$$

where c_k are the components of the eigenvector and the complex structure z is associated with the natural metric. We will investigate how the cutoff might affect the eigenstate.

Since the eigenstate is represented as an antiholomorphic polynomial completely determined by its roots, our idea is to characterize the eigenstate from the perspective of the distribution of its roots on the complex plane. The algorithm that is used to find the roots is called Jenkins-Traub algorithm[35]. The basic idea is as follows. Consider a polynomial

$$P(z) = z^n + a_{n-1}z^{n-1} + \cdots + a_1 z + a_0 = \prod_{j=1}^{p}(z-\alpha_j)^{m_j} \tag{3.6}$$

where the a_i are complex numbers with $a_0 \neq 0$. The zero α_j has multiplicity $m_j, j = 1, \ldots, p$ so that $\sum_{j=1}^{p} m_j = n$. We have

$$P'(z) = \sum_{j=1}^{p} m_j P_j(z), \tag{3.7}$$

$$P_j(z) = \frac{P(z)}{z-\alpha_j}. \tag{3.8}$$

Generate a sequence of polynomials $H^{(\lambda)}(z)$ starting with $H^{(0)}(z) = P'(z)$, each of the form

$$H^{(\lambda)}(z) = \sum_{j=1}^{p} c_j^{(\lambda)} P_j(z), \tag{3.9}$$

and the goal is to let $H^{(\lambda)}(z) \to c_1^{(\lambda)} P_1(z)$, then a sequence $\{t_\lambda\}$

$$t_{\lambda+1} = s_\lambda - \frac{P(s_\lambda)}{\tilde{H}^{(\lambda+1)}(s_\lambda)}, \tag{3.10}$$

$$\tilde{H}^{(\lambda)}(z) = \frac{H^{(\lambda)}(z)}{\sum_{j=1}^{p} c_j^{(\lambda)}}, \tag{3.11}$$

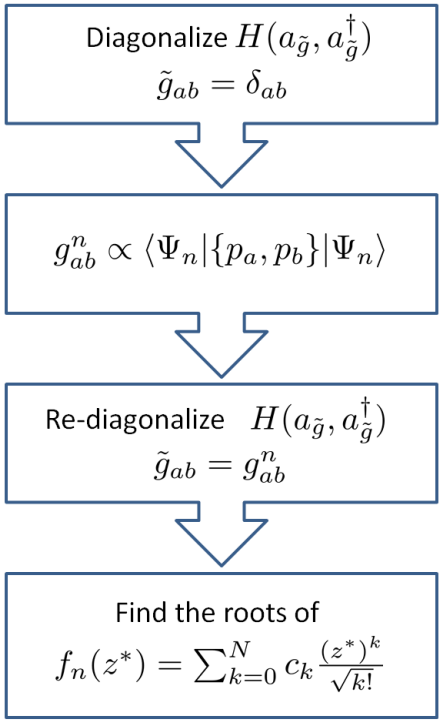

Figure 3.1: Diagram of numerical procedures. The Hamiltonian is diagonalized with the Landau-orbit metric identical to the Euclidean metric. After the natural metric for a specific Landau level indexed by n is calculated, diagonalize the Hamiltonian for a second time using that metric to define a and $a^\dagger$. The roots of the polynomial part of the nth eigenstate (which is in nth Landau level) are then found using Jenkins-Traub algorithm. For another Landau level $n' \neq n$, restart from the second step.

where s_λ is an arbitrary sequence, approaches $s_\lambda - (s_\lambda - \alpha_1) = \alpha_1$. The $H^{(\lambda)}(z)$ are generated by the formula

$$H^{(\lambda+1)}(z_\lambda) = \frac{1}{z - s_\lambda} \left(H^{(\lambda)}(z) - \frac{H^{(\lambda)}(s_\lambda)}{P(s_\lambda)} P(z) \right) \tag{3.12}$$

$$= \frac{P(z)}{z - s_\lambda} \sum_{j=1}^{p} c_j^{(\lambda)} \left(\frac{1}{z - \alpha_j} - \frac{1}{s_\lambda - \alpha_j} \right)$$

$$= \sum_{j=1}^{p} \frac{c_j^{(\lambda)}}{\alpha_j - s_\lambda} P_j(z). \tag{3.13}$$

If we choose s_λ so that it approaches α_1 (*e.g.*, let $s_\lambda = t_\lambda$) we will achieve our goal.

A practical problem in the process described above is that the factor $1/\sqrt{k!}$ present in Eq.(3.5) decays so fast that at $k \sim 170$ it already reaches the limit of double-precision floating-point format. To achieve a higher cutoff, we used the arbitrary-precision data type provided by the GMP library in the root-finding algorithm. We also needed to transform the LAPACK routines used for diagonalization into arbitrary-precision versions and we found an open-source package called MPACK[32] that suited our purpose.

3.2 Topological spin

In this section we will present numerical results, particularly the distribution of complex roots for a guiding-center coherent state. An important concept dubbed a *topological spin* will be introduced to characterize different Landau levels.

Before jumping into the details, let's get some taste from a benchmark case where we calculate the roots of an expansion of the modified Bessel function of the first kind

$$I_0(2z) = \sum_{k=0}^{N} \frac{1}{(k!)^2} z^{2k}. \tag{3.14}$$

To mimic the C_4 symmetry of a pure quartic term, we will use $I_0(2z^2)$ instead. The function $I_0(z)$ has inversion symmetry $I_0(z) = I_0(-z)$ and all its zeros lie on the imaginary axis. Therefore the zeros of $I_0(2z^2)$ should be aligned on four rays emanating from the origin with arguments $\pm\pi/4$ and $\pm 3\pi/4$. Fig.(3.2) verifies this (along with numerical artifacts).

We will start with class I quartic case (for the definition of the four classes, see Sec.(2.4)). A typical layout of the roots is presented in Fig.(3.3). The central zeros are organized in a cross shape due to the C_4 symmetry. There are n mod 4 degenerate roots at the origin where n is the Landau-level index, and the degeneracy will be lifted once we add quadratic terms to the Hamiltonian (as the C_4 symmetry is broken). The

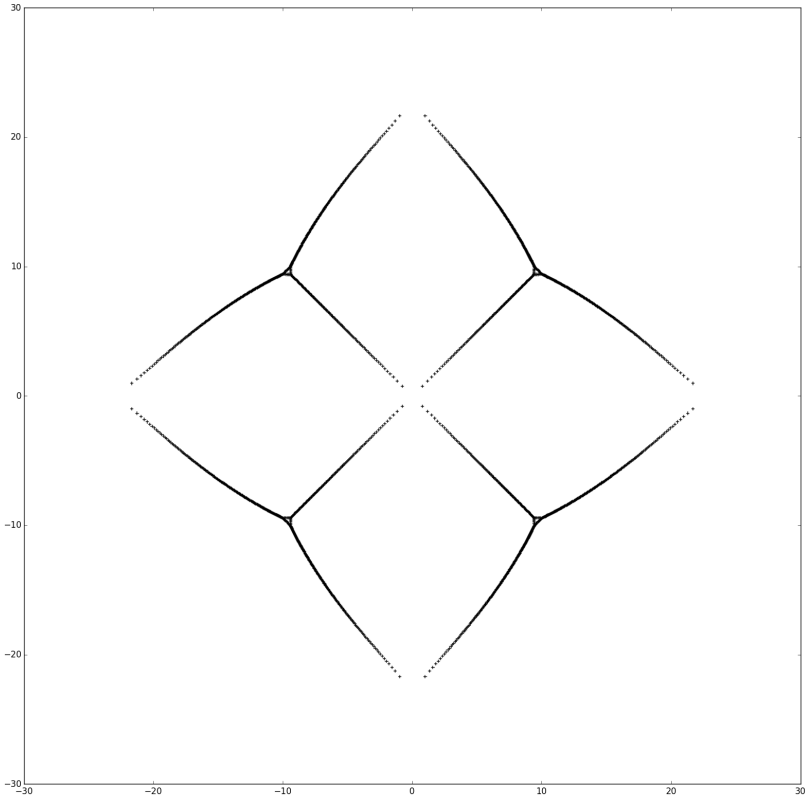

Figure 3.2: Roots of an expansion of $I_0(2z^2)$ at cutoff $N = 500$. The four rays of roots at arguments $\pm\pi/4$ and $\pm 3\pi/4$ are true roots while the arcs on the outside are due to a finite cutoff and will be pushed further outward when the cutoff increases.

feature that also appears in the benchmark case is the presence of four "spikes" that point to the origin at ± 45 and ± 135 degrees. The new features are the regions with quasi-uniform 2D distributions bounded by lines of roots also with nearly constant density. The precise locations of the roots inside those 2D regions are sensitive to perturbation of the Hamiltonian, but we believe the very existence of such "dark" areas is universal.

Note that there are also truncation-dependent features tied to the boundary $|z| \approx R_N$, where N is the cutoff, but the structure for $|z| \ll R_N$ becomes independent of N as it, and consequently R_N, is increased, as illustrated in Fig.(3.4). We

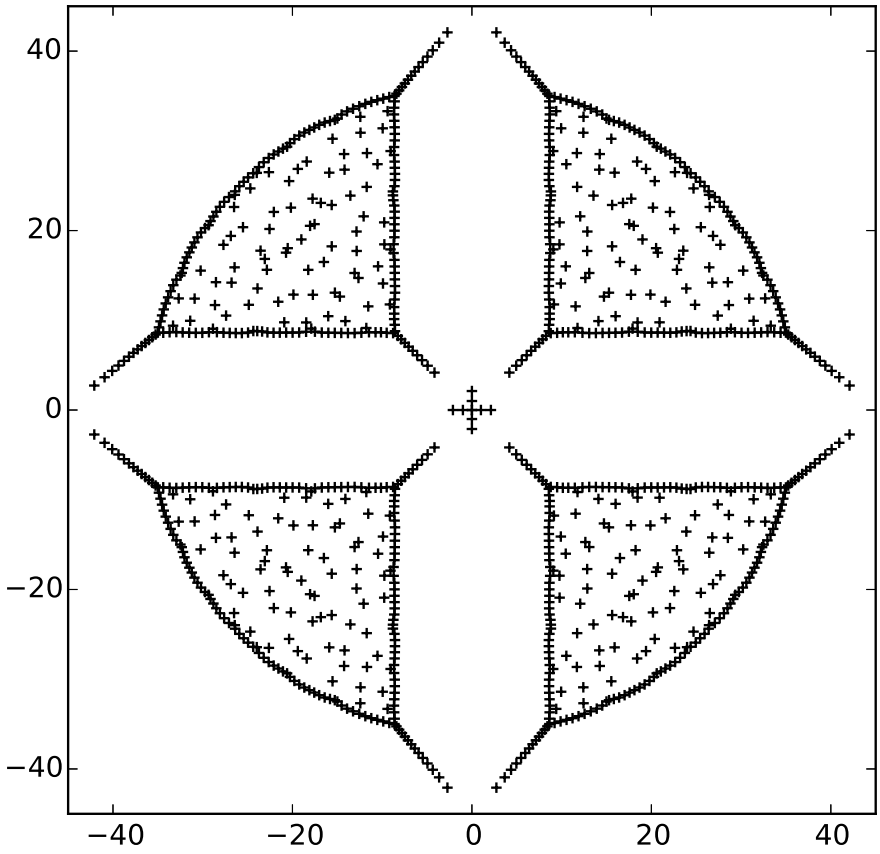

Figure 3.3: Root distribution on the complex plane of the coherent state in the 10th Landau level for class I quartic term in Eq.(2.45) with $c-1=4$ at a truncation of 500 even-parity states. Ten central zeros, with two being degenerate at the origin, form a cross due to the C_4 symmetry. The peripheral zeros also have interesting features, such as four "spikes" pointing to the origin and line charges with constant density that bound 2D regions of quasi-uniform distributions. The arcs on the boundary are generated due to finite truncation and should not be regarded as part of the zero pattern.

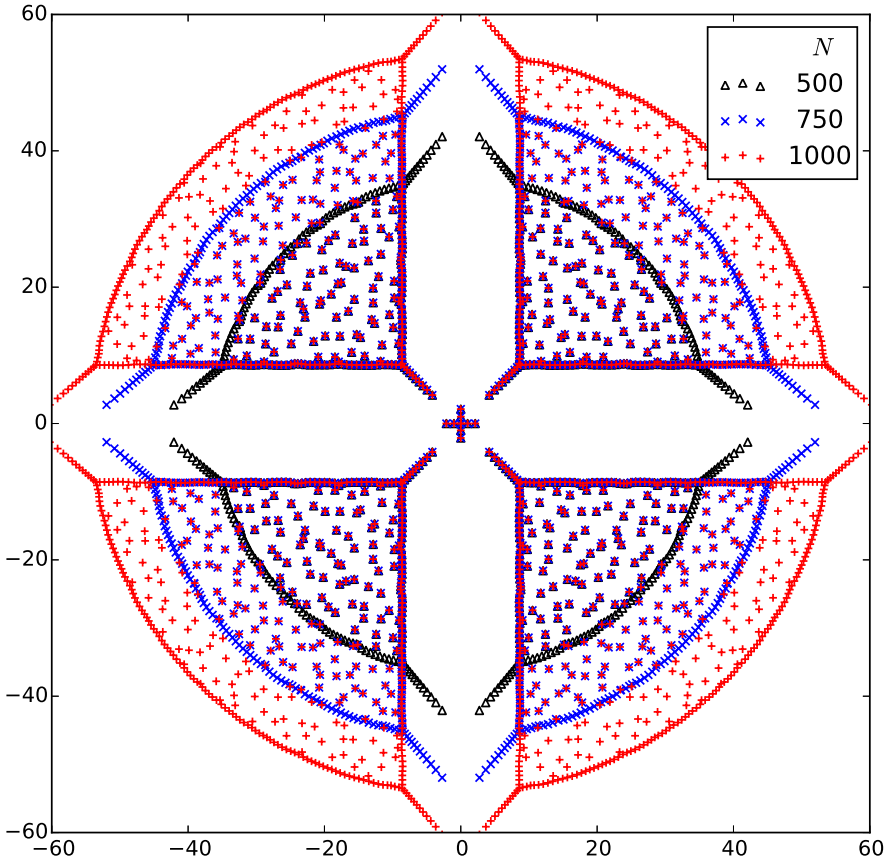

Figure 3.4: Root distribution on the complex plane of the coherent state in the 10th Landau level for class I quartic term in Eq.(2.45) with $c-1=4$ at a truncation of 500, 750 and 1000 even-parity states. For each N, we used a sufficiently high precision in diagonalization so that further increasing the precision would not do any better in terms of the locations of the zeros. As N increases, the region covered by the zeros expands. However, the existing pattern of zero distribution doesn't change, which justifies the validity of our results.

therefore believe that this calculational method reveals the true structure of roots of the antiholomorphic non-polynomial function $f_n(z^*)$ in a range $|z| < R$ that can be increased at will at the expense of increasing the floating-point precision of the numerical diagonalization.

Let's now look at other features of the distribution. There is a 2D electrostatic analogy by interpreting

$$\ln|\Psi_n|^2 = 2\sum_{k=0}^{N} \ln|z - z_k| - z^* z + const., \tag{3.15}$$

where z_k are the roots, as the Coulomb potential at z of a 2D distribution of charges located at the roots and a neutralizing background charge density $1/\pi$ (if each root carries a unit charge). To visualize that, we show in Fig.(3.5) the contours of $\ln|\Psi_n|^2$. We see piecewise segments with different curvatures as the 2D regions change effective background charge density and the linear alignments of roots act as branch cuts. Notice the "volcano crater" at the center enclosed by an annulus-like region containing local maxima and saddle points. The free parameter $c-1$ controls the shape of the annulus. A simple calculation reveals that $c-1 > 2$ corresponds to a concave shape, while $c-1 < 2$ convex. This annulus is a fattened version of the semiclassical orbit. Actually if we define a "ridge" inside the annulus as the boundary between two regions where the gradient field flows toward either the origin or infinity (the local maxima and the saddle points are all right on the boundary), as shown in Fig. (3.6), we find that the area enclosed by that ridge is exactly πn with n being the Landau level index, which corresponds to an area of $2\pi\hbar eBn$ on the momentum plane. This is just the Bohr-Sommerfeld quantization mentioned in Sec.(2.3) shifted by a constant.

To obtain an intuitive understanding of the structure, recall that in the rotationally invariant case, $\Psi_n \propto (z^*)^n \exp(-\frac{1}{2}z^* z)$ has n zeros at the origin, a ring of maxima at a radius of $\sqrt{n}$ and a Gaussian tail extending to infinity. With a moderate per-

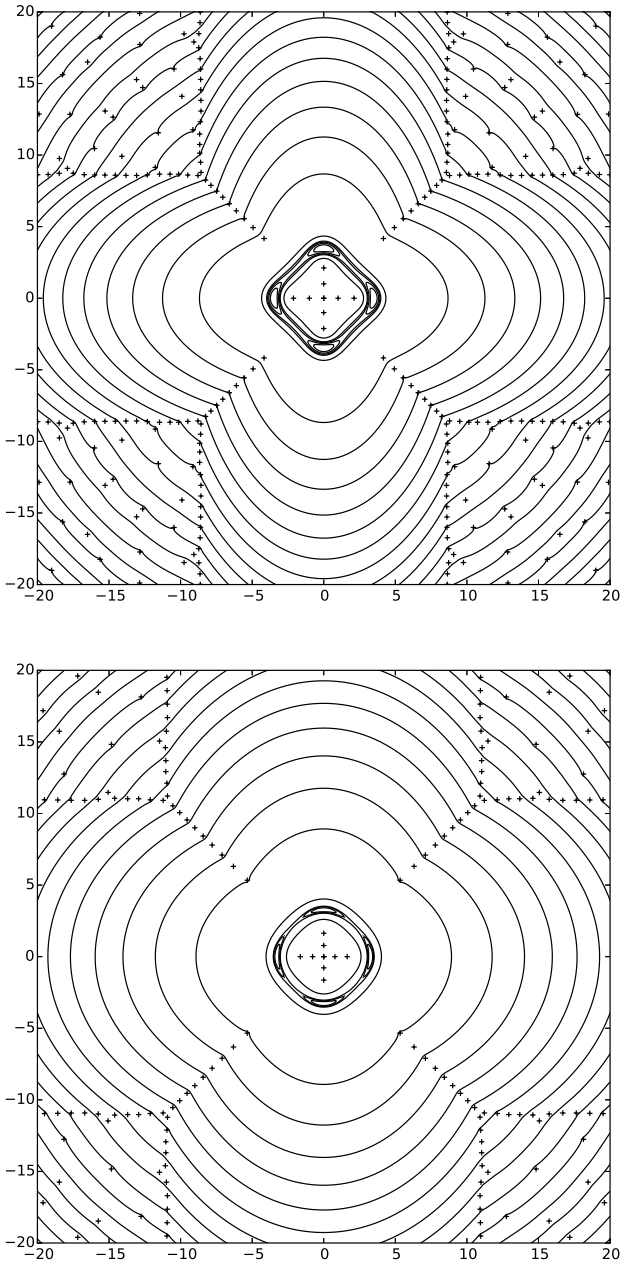

Figure 3.5: Contour plots of $\ln|\Psi_{10}(z,z^*)|^2$ where $\Psi_{10}(z,z^*)$ is the coherent state in the 10th Landau level for class I quartic term (2.45) with $c-1=4>2$ (top) and $c-1=1<2$ (bottom). Both plots show piece-wise contours with the four spikes and the line charges as branch cuts. Another common feature is the existence of four maxima along the directions of the central cross and four saddle points along those of the spikes. Despite the similarities, the two plots also show qualitatively different shapes of the semiclassical orbits. We see that $c-1>2$ corresponds to concave shapes while $c-1<2$ to convex ones.

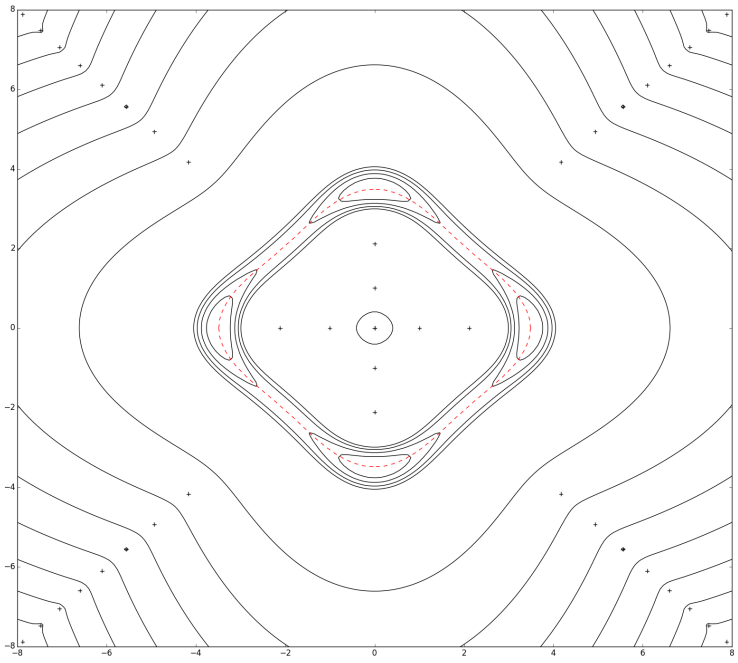

Figure 3.6: A "ridge" (dashed) defined as the boundary between two regions where the gradient field flows to the origin (inside) or infinity (outside). The roots are those of the coherent state in the 10th Landau level for class I quartic term with $c-1=2$. Contours are also shown. Notice that the local maxima and the saddle points are all right on the ridge. The area enclosed by the ridge is πn, corresponding to an area of $2\pi\hbar eB$ on the momentum plane, which is consistent with (shifted) semiclassical quantization.

turbation that breaks rotational invariance, the new zeros will only appear where the original wavefunction has a small amplitude, namely, around the origin or along the Gaussian tail separated by the peak in between which contains most of the weight of the wave function. In Fig.(3.7) we show that the peak region can encompass as much as 90 percent of the total weight.

The existence of a clean separation between the central zeros and the rest of the pattern by an annulus-like region, or more rigorously a region with Euler characteristic $\chi = 0$, defined by $|\Psi_n| \geq V, V \in \mathbb{R}^+$, is critical for our definition of a topological spin,

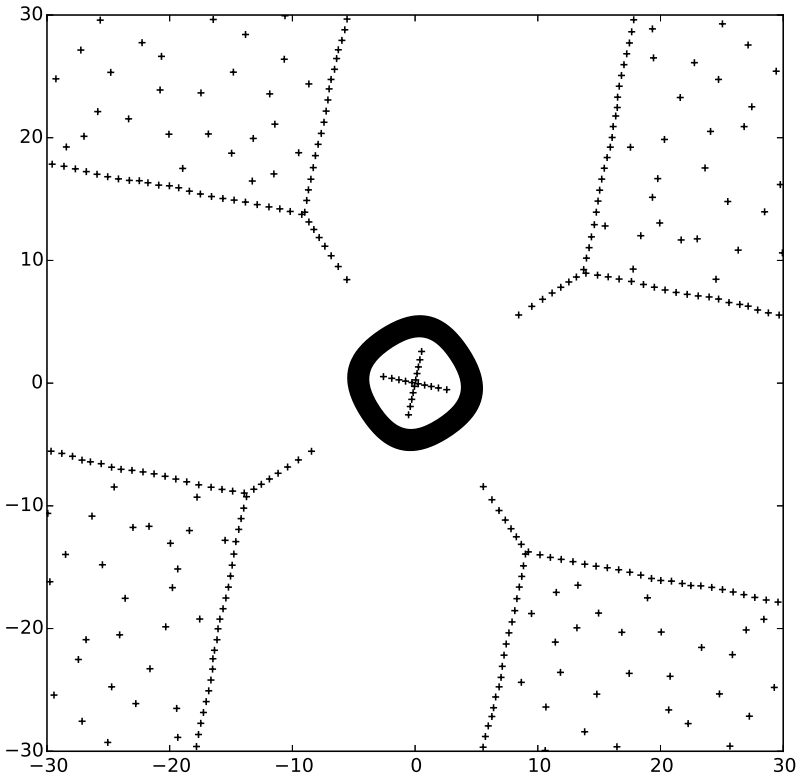

Figure 3.7: Black region accounting for 90 percent of the total weight (probability) of $|\Psi_{20}|^2$, the coherent state in the 20th Landau level of the Hamiltonian $p_x^2 + p_y^2 + 2p_x^4 + 3p_y^4 + 4\{p_x^2, p_y^2\} + \{p_x, p_y^3\}$. The annulus is bounded by contours at the same value of the amplitude $|\Psi_{20}|$ and cleanly separates the central zeros from the rest of the structure.

which is

$$s_n = n + \tfrac{1}{2} \tag{3.16}$$

where n is the number of central zeros. Now we can provide a more convincing justification for the natural metric used to define the coherent states. If we deform the metric, at some point the central zeros will leak out of the "crater" region and the coherent state doesn't have a semiclassical counterpart anymore. An example is shown in Fig.(3.8) where the guiding-center metric is chosen to be δ_{ab} even though

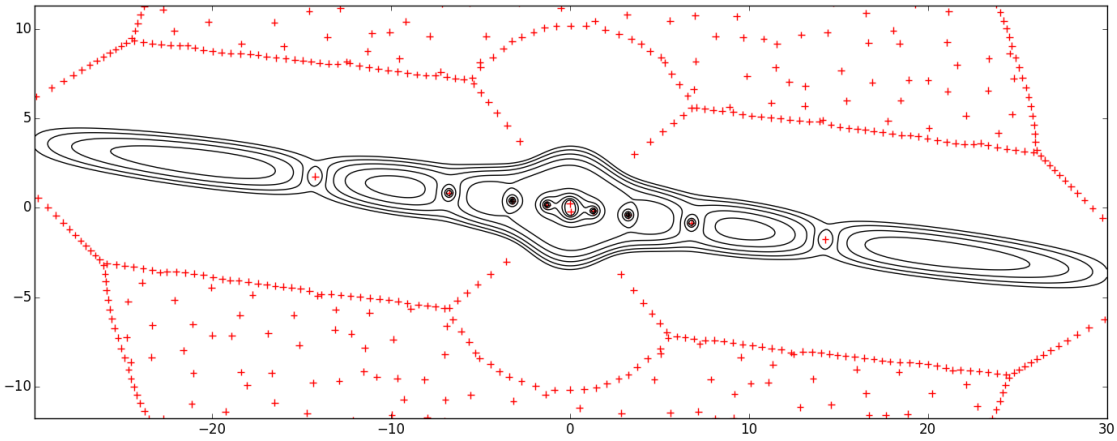

Figure 3.8: Contours of $\ln|\Psi_{10}(z,z^*)|^2$, a coherent state in the 20th Landau level with the guiding-center metric $\bar{g}_{ab}$ equal to the Euclidean metric δ_{ab} while the natural metric is extremely squeezed, which can be told from the elongated distribution of the central roots and the contours. Those roots are no longer separated from the outer ones by an annulus-like region defined by $|\Psi_{10}(z,z^*)| > V$ where V is a constant. Instead, they are divided into subgroups by those local maxima.

the natural metric is in a extremely elongated shape. The central zeros can not be enclosed by a region that meets our requirements.

Let's briefly look at the other three classes of pure quartic term. As mentioned in Sec.(2.4) the classical orbits for the three classes are not closed. Although the noncommutativity of p_a gives rise to effective quadratic terms for classes II and III, thus closing the quantum orbits, we expect that a clean separation of the central zeros *cannot* be achieved for any of the three classes, which is verified in Fig.(3.9).

We now combine quartic terms with quadratic terms. We adopt a different parametrization here

$$\begin{aligned} H = & Ap_x^2 + Bp_y^2 + Cp_x^4 + Dp_y^4 \\ & + E\{p_x^2, p_y^2\} + F\{p_x, p_y^3\} + G\{p_x^3, p_y\}. \end{aligned} \tag{3.17}$$

The C_4 symmetry generically breaks down. However, as we go to high-energy states, the quartic terms will eventually dominate and therefore a quasi-C_4 symmetry will

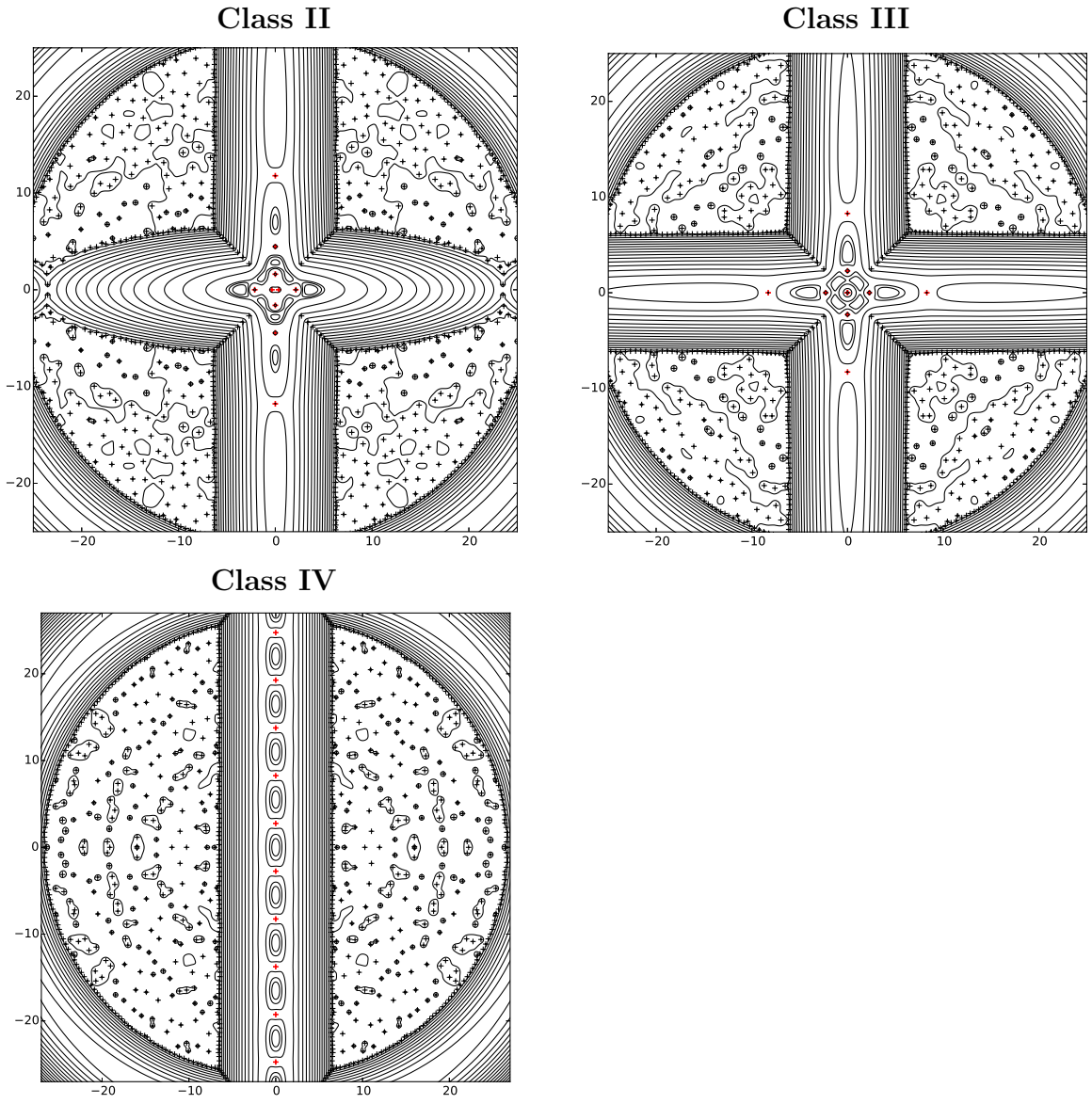

Figure 3.9: Contour plots of $\ln|\Psi_{10}(z,z^*)|^2$, where $\Psi_{10}(z,z^*)$ is the coherent state in the 10th Landau level, for class II-IV quartic terms, with the Hamiltonian being $\{p_x^2, p_x^2+p_y^2\}$, $\{p_x^2, p_y^2\}$, p_x^4 respectively. Although classes II&III have closed contours that enclose part of the central zeros (red pluses), none of the three has a clean separation between all the central zeros and the rest ones. The contours inside the 2D-distribution regions also demonstrate qualitatively different features from those of class I : the puddle-like shapes indicate uniformly vanishing amplitudes.

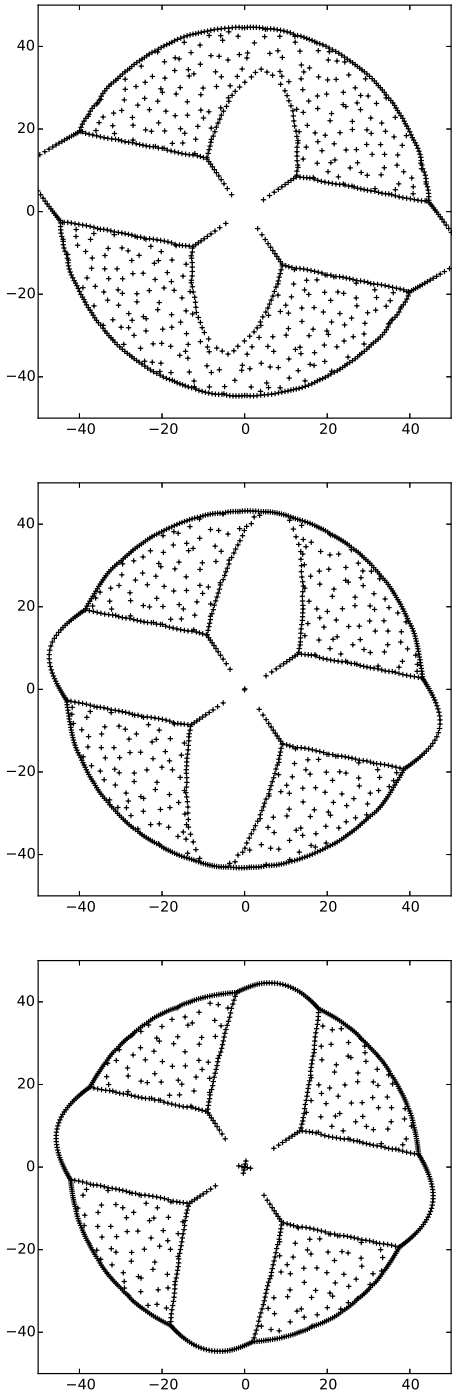

Figure 3.10: Root distribution on the complex plane of the coherent states in the (from top to bottom) 0th, 2nd and 10th Landau level. The Hamiltonian assumes the form $20p_x^2 + 20p_y^2 + 2p_x^4 + 3p_y^4 + 4\{p_x^2, p_y^2\} + \{p_x, p_y^3\}$. As the Landau level index n increases, the C_4 symmetry gradually restores as quartic terms dominate.

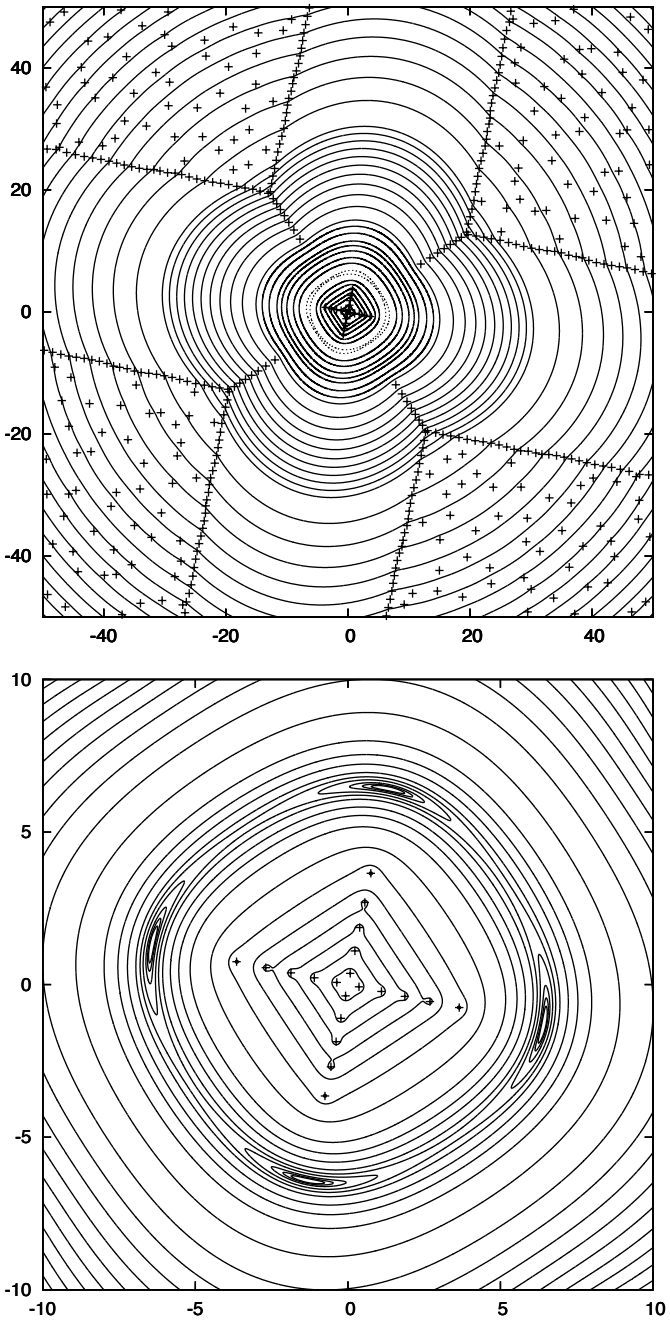

Figure 3.11: Contour plots of $\ln|\Psi_{20}|^2$ where Ψ_{20} is the coherent state in the 20th Landau level of the Hamiltonian $p_x^2 + p_y^2 + 2p_x^4 + 3p_y^4 + 4\{p_x^2, p_y^2\} + \{p_x, p_y^3\}$. The lower plot is a zoom-in on the central region. The contours have the same piece-wise structures as in the case of pure quartic terms. Also note that the central cross still points to the maxima and that the spikes to the saddle points.

gradually appear as the Landau index n increases, as shown in Fig.(3.10). Due to this asymptotic C_4 symmetry, the generic features of the root structure and the contours still hold for a mixture of quadratic and quartic terms, as illustrated in Fig.(3.11).

To make connection with the usual Galilean theory, we remark that as we reduce the weights of the quartic terms, the central zeros will shrink toward the origin and the outer zeros will be pushed toward infinity (but the overall pattern doesn't change), consistent with the fact that at the limit of a pure quadratic term $f_n(z^*)$ becomes a monomial $(z^*)^n$ whose roots all sit at the origin.

3.3 The "shift"

The topological spin introduced in the previous section is related to a topological quantity called the "shift" $\mathcal{S}$ that was first defined by Wen and Zee[43] in the relation between the number of electrons N_e and the number of flux quanta N_ϕ on a manifold with Euler characteristic χ,

$$N_\phi = \nu^{-1} N_e - \mathcal{S}\chi/2. \tag{3.18}$$

The relation between the topological spin and the shift for the IQHE is

$$\sum_n \nu_n s_n = \mathcal{S}/2. \tag{3.19}$$

The Euler characteristic is a topological invariant related to the genus, another topological invariant counting the number of "handles" in a closed orientable 2D manifold, by

$$\chi = 2 - 2g. \tag{3.20}$$

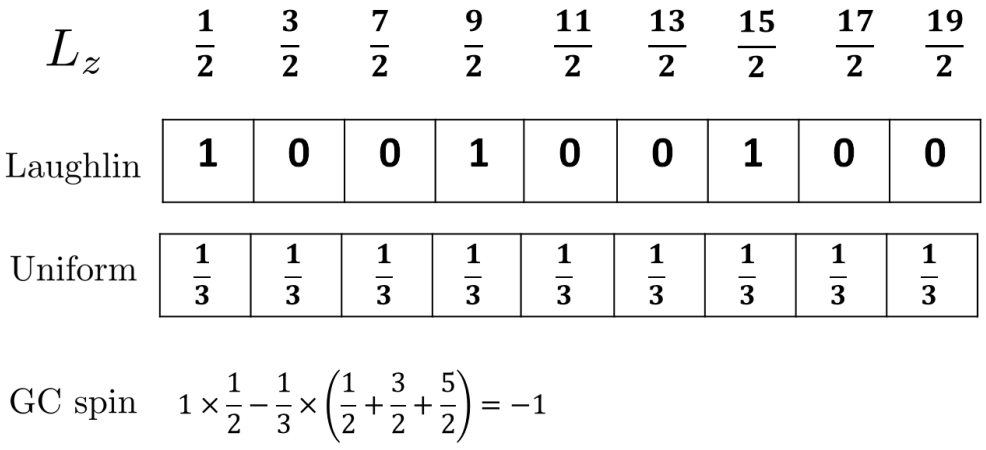

Figure 3.12: Demonstration of calculation of the guiding-center spin for Laughlin 1/3 state. Each composite boson is a 100 segment, and the guiding-center spin is defined as the difference between the angular momentum of a composite boson to that of a uniformly distributed droplet, in this case $\frac{1}{3}\frac{1}{3}\frac{1}{3}$.

For example, a sphere has $g = 0$ and $\chi = 2$, so the nth Landau level will have $2s_n = 2n + 1$ extra orbitals. The exact spectrum was first calculated by Haldane[17], who showed that the orbitals in the nth Landau level on the sphere with a charge-$2S$ magnetic monopole sitting at the center can be represented by a spin $S + n$ object, *i.e.*, the degeneracy is $2(S + n) + 1 = 2S + (2n + 1)$. Another examples is the 2D torus. It has $g = 1$ and $\chi = 0$, and therefore the number of available orbitals is still equal to N_ϕ. The first exact calculation was by Haldane and Rezayi[20].

For the FQHE, the shift has another contribution coming from the guiding-center degree of freedom. The guiding-center spin is defined as the residual angular momentum of a composite boson with respect to a uniform distribution of electrons. See Fig.(3.3).

An explanation from the perspective of the effective theory is that the topological spin couples to the Gaussian curvature of the underlying manifold and it is the total effective curvature combining the magnetic field ($U(1)$ curvature) and the Gaussian curvature that determines the number of available orbitals, as illustrated in Fig.(3.3).

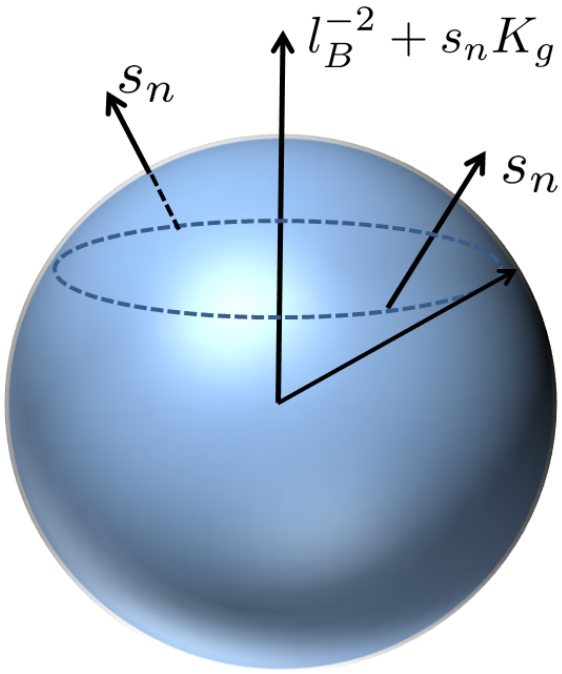

Figure 3.13: The effective curvature for a topological spin s_n moving on the sphere with a Gaussian curvature K_g. The effective curvature consists of the magnetic field (curvature of U(1) gauge fields) with coupling constant $e/\hbar$ and the Gaussian curvature (curvature of the spin connection) with coupling constant s_n.

The Gauss-Bonnet theorem states that

$$\int_M K dA = 2\pi\chi(M), \tag{3.21}$$

i.e., the integral of the Gaussian curvature K over a closed 2D manifold M is equal to its Euler characteristic $\chi(M)$. As a result, there will be $s_n\chi$ extra orbitals in the nth Landau level. However, the Gaussian curvature doesn't need to be that of the underlying manifold. In his geometrical description of the QHE, Haldane[19] pointed out that even on a flat manifold there can be Gaussian curvature due to a spatially varying guiding-center metric that minimizes local interaction.

We have seen that the topological spin is a well-defined topological quantity. In the next chapter where we reformulate the Hall viscosity, we will show that the usual identification between the scalar viscosity, a non-topological quantity, and the shift (or equivalently the topological spin) is only a coincidence at the presence of rotational symmetry and should not be treated as a fundamental identity.

3.4 Nevanlinna theory

In this section we would like to revisit the problem of diagonalizing the Hamiltonian but from the perspective of solving a complex differential equation. Using the complex representation for a and $a^\dagger$ in Eq.(2.36) and the parametrization for the Hamiltonian in Eq.(2.45) the eigen-problem

$$H|\Psi\rangle = E|\Psi\rangle \tag{3.22}$$

can be written as a fourth order complex differential equation on the antiholomorphic part of the wavefunction:

$$\begin{aligned}
&(\partial_{z^*}^4 + \alpha_2(z^*)\partial_{z^*}^2 + \alpha_1(z^*)\partial_{z^*} + \alpha_0(z^*))f(z^*) = 0,\\
&\alpha_2 = -(2 + \frac{8}{c-1})z^{*2},\\
&\alpha_1 = -(4 + \frac{16}{c-1})z^*,\\
&\alpha_0 = z^{*4} - 1 - \frac{2}{c-1}(1 - \frac{E}{E_0}).
\end{aligned} \tag{3.23}$$

In the mathematical literature Nevanlinna theory has been applied to the study of global properties of solutions of complex differential equations[27]. One critical result is that for a complex differential equation of any order with the coefficients being entire functions of z (holomorphic functions at all finite points over the whole complex plane), the solutions are guaranteed to be entire functions. This nice property justifies our power-expansion method in the numerical analysis.

To look at the theory in more detail we need to introduce several concepts. Let f be a meromorphic function not identically equal to 0. Let $n(r, f)$ (the unintegrated counting function) denote the number of roots $f(z) = 0$ in $|z| \leq r$, each root according to its multiplicity. We define (the counting function)

$$N(r, f) \equiv \int_0^r \frac{n(t, f) - n(0, f)}{t} dt + n(0, f) \log r, \tag{3.24}$$

and (the proximity function)

$$m(r, f) \equiv \frac{1}{2\pi} \int_0^{2\pi} \log^+ \left| \frac{1}{f(re^{i\varphi})} \right| d\varphi, \tag{3.25}$$

$$\log^+ \alpha \equiv \max(0, \log \alpha).$$

The counting function measures how the number of roots grows with r while the proximity function calculates the average of $\log^+ |1/f|$ on a circle with radius r. Then the characteristic function is defined as

$$T(r, f) \equiv m(r, f) + N(r, f), \tag{3.26}$$

which leads us to a very important quantity called the order of a meromorphic function,

$$\sigma(f) \equiv \limsup_{r \to \infty} \frac{\log T(r, f)}{\log r}. \tag{3.27}$$

If f is also an entire function, by Liouville's theorem it is either unbounded or constant. Excluding the constant case, we would generically expect $m(r, f) \to 0$ as $r \to \infty$ and the characteristic function is dominated by the counting function, so the order is the exponent in the power law $N(r, f) \sim r^\sigma$. Notice that $1/f$ is also a meromorphic function, and the corresponding functions $n(r, 1/f), N(r, 1/f)$ and $T(r, 1/f)$

can be defined. The first main theorem states that

$$T(r, 1/f) = T(r, f) + O(1), \tag{3.28}$$

which implies that f and $1/f$ have the same order. For an entire function f, $1/f$ doesn't have roots at finite points, so $N(r, 1/f) \equiv 0$ and $T(r, 1/f) \equiv m(r, 1/f)$. Now the order appears in $\log^+ |f| \sim r^\sigma$. We see that the asymptotic growth of an entire function is closely related to that of the number of its roots.

For an nth order complex differential equation

$$f^{(n)} + a_{n-1}(z)f^{(n-1)} + \cdots + a_1(z)f' + a_0(z)f = 0 \tag{3.29}$$

with the coefficients being entire functions, the possible orders for the solutions are rational numbers. If the coefficients are polynomials

$$a_j(z) = \sum_{i=0}^{\alpha_j} c_{ij} z^i, \quad j = 0, \ldots, n-1, \tag{3.30}$$

then the order satisfies

$$\sigma(f) \leq 1 + \max_{j=0,\ldots,n-1} \frac{\alpha_j}{n-j}. \tag{3.31}$$

Let's look at our case. Notice that the operators a and $a^\dagger$ are linear in z^* and ∂_{z^*}, which means the total power of z^* and ∂_{z^*} is at most n where n is the highest order term in the Hamiltonian (n=4 for a quartic Hamiltonian). This is equivalent to the following inequality

$$\alpha_j + j \leq n, \tag{3.32}$$

which says

$$\sigma(f) \leq 2. \tag{3.33}$$

This means the counting function $N(r, f)$ can not grow faster than r^2 (in our numerical case it appears to grow as r^2) or $log^+|f|$ can not grow faster than r^2, which is consistent with the fact that $f(z^*) \exp -\frac{1}{2} z^* z$ is a normalizable wavefunction.

Chapter 4

Hall viscosity

In the previous chapter we looked at the topological property of the guiding-center coherent states. From this chapter on, we will start to investigate generic response functions in the absence of Galilean or rotational symmetry. In particular, this chapter is devoted to the study of the Hall viscosity, linear response of the stress tensor to a non-uniform flow velocity field. We will have an overview of viscosity in a classical fluid and in a quantum Hall fluid. Then by clarifying the definition of the stress tensor as variation of an action against a strain field, we present a generic formula for the Hall viscosity that forfeits the concept of "intrinsic orbital angular momentum" as interpreted in previous work.

4.1 Viscosity

The viscosity of a fluid is the linear response of its stress tensor $T^a_{\ b}$ (current-density of momentum) to a non-uniform flow velocity field v^a

$$T^a_{\ b}(\boldsymbol{x},t) = \eta^{a\ c}_{\ b\ d}(\boldsymbol{x},t)\partial_c v^d(\boldsymbol{x},t) + O(v^2). \tag{4.1}$$

Notice that we have differentiated between covariant (lower) and contravariant (upper) indices, which is essential in clarifying the structure of the viscosity tensor at the absence of rotational invariance. Both the stress tensor T^a_b and the viscosity tensor $\eta^{a\,c}_{b\,d}$ are locally-defined (implying they should not be related to any topological quantity) mixed-index tensors. The stress tensor appears in the equation of conservation of momentum density T^0_a (assuming the system preserves translational invariance)

$$\partial_t T^0_a + \partial_b T^b_{\ a} = 0, \tag{4.2}$$

and it is clear that the stress tensor should be a (1,1) tensor.

The viscosity for a classical fluid is usually associated with its "thickness" or "viscousness" (for example, honey has a much higher viscosity than water), as it measures the internal resistance or friction against relative motion between different parts of the fluid and is a source of dissipation of energy, as shown in Fig.(4.1). In the next section we will investigate the viscosity in a QHE system. It has the amazing property of being dissipationless and is given the name "Hall viscosity".

4.2 Hall viscosity

The commonly studied (integer or fractional) quantum Hall systems are gapped incompressible fluids. To be more specific, there are two types of gaps (mentioned in Sec.(1.2)), one for charged excitations and one for neutral excitations. For IQHE, they are both in the order of the inter-Landau-level energy $\hbar\omega_c$. For FQHE, the (gapped) charged excitation is a complex object called a quasiparticle that has fractional charge and fractional statistics in the Laughlin series[29] while the neutral excitation is the well-known magneto-roton mode first proposed by Girvin, MacDonald and Platzman[13], which is interpreted as a dipole consisting of a quasihole and a quasiparticle. Fig.(4.2) shows the spectrum for filling 1/3.

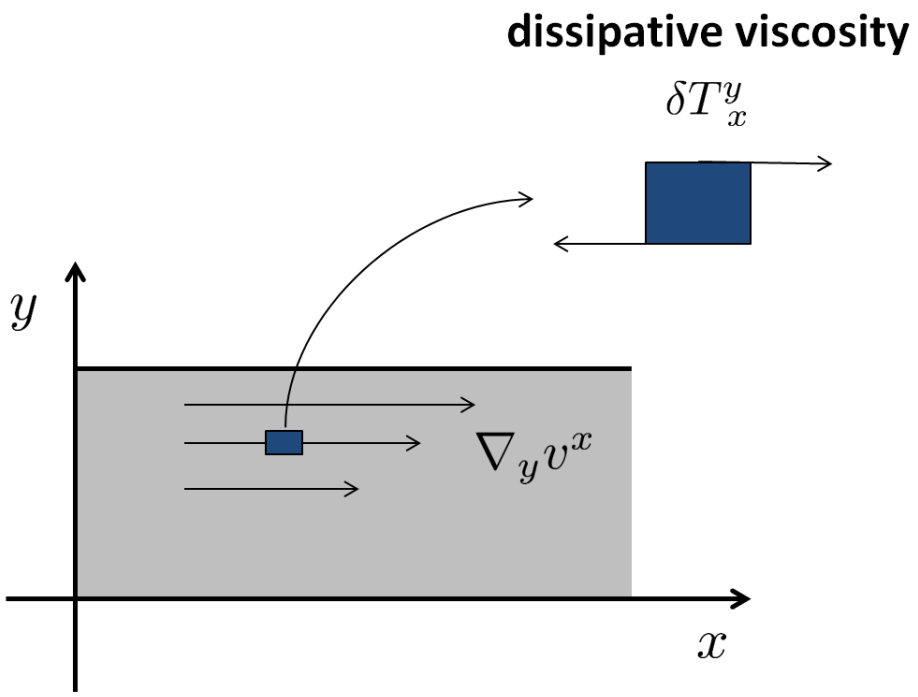

Figure 4.1: Classical viscosity associated with dissipation. There is a gradient in the y direction for a velocity field that flows in the x direction. The viscosity gives rise to a shear stress that acts as a friction between layers of different velocities and the fluid appears "viscous", hence the name.

It's the gap for neutral excitations that is of concern here. The presence of such a gap forbids transmission of forces or dissipation of energy through the bulk. A viscosity that satisfies the dissipationless property is called the Hall viscosity and can only exist when time-reversal symmetry is broken. A typical configuration is shown in Fig. (4.3). The mathematical expression for the condition is

$$T^b_a \partial_b v^a = 0, \tag{4.3}$$

or equivalently the viscosity tensor $\eta^{a\,c}_{b\,d}$ must be antisymmetric under permutation $a, b \leftrightarrow c, d$

$$\eta^{a\,c}_{b\,d} = -\eta^{c\,a}_{d\,b}. \tag{4.4}$$

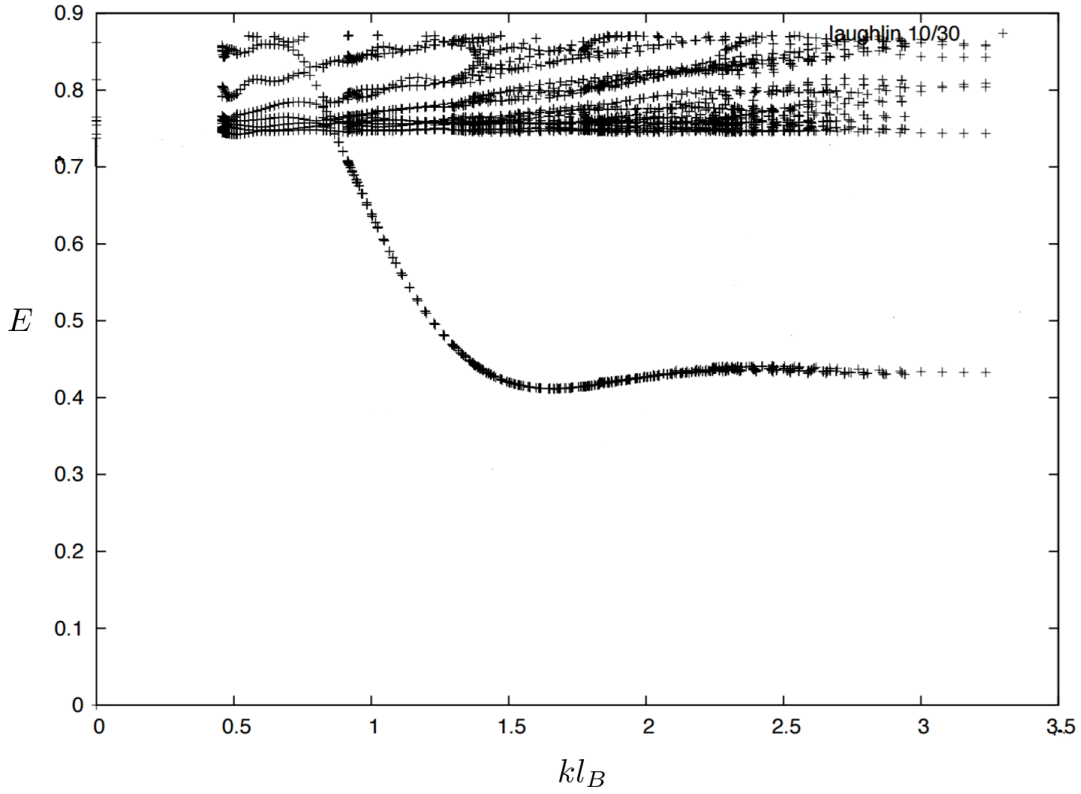

Figure 4.2: Spectrum of 10 electrons in 30 orbitals on the torus with V_1 pseudopotential interaction. The Laughlin ground state is set at the origin (zero momentum and zero energy). The magneto-roton mode merges into the multi-roton continuum in the long wavelength limit. The roton-minimum defines the gap for a FQHE system. (Plot courtesy: F. D. M. Haldane).

The fact that there is no transmission of forces implies that a quantum Hall fluid does not support a hydrostatic pressure. An external force acting upon the edge will only modify the velocity of the edge currents and have no impact on the bulk, as illustrated in Fig.(4.4). Since pressure is the trace of the stress tensor, this dictates the traceless condition

$$T^a_a = 0. \tag{4.5}$$

Note that a gapped quantum incompressible fluid is quite different than a classical incompressible liquid. The incompressibility of a classical liquid is just a thought-

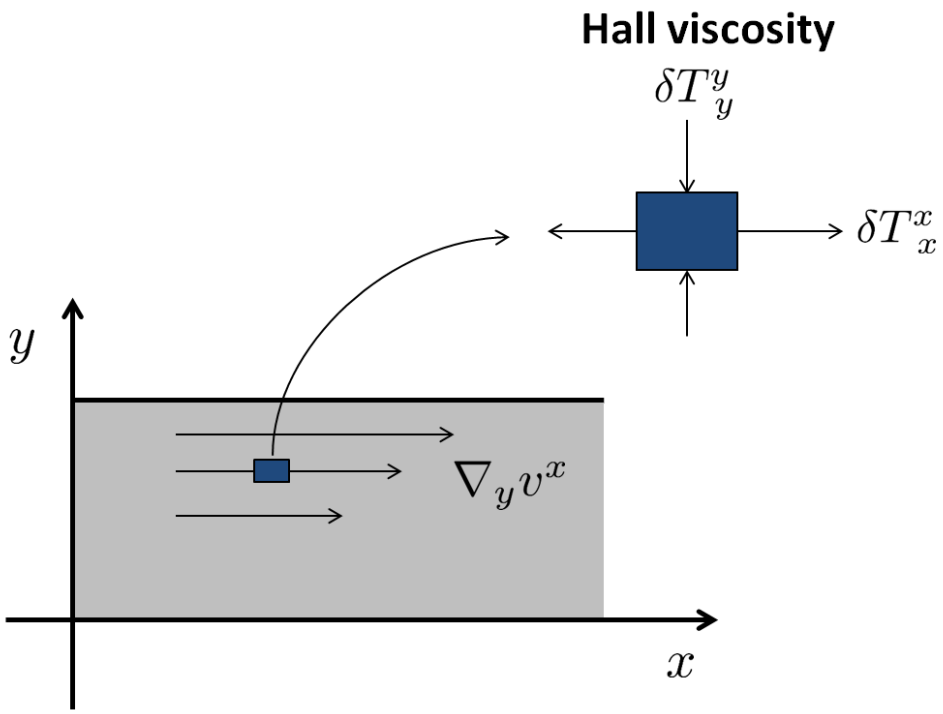

Figure 4.3: Hall viscosity for a velocity field that flows in the x direction with a gradient in the y direction . The stress on the top and bottom surfaces is perpendicular to the flow velocity and therefore there is no dissipation of energy. The stress tries to deform the local fluid while preserving the area, *i.e.*, it is traceless.

experiment where we send the sound-wave velocity to infinity. The consequence is that the liquid supports a hydrostatic pressure that is instantaneously uniform throughout the liquid. In contrast, a quantum Hall fluid doesn't support sound waves due to the presence of a gap for collective excitations.

These two constraints (dissipationlessness and tracelessness) significantly reduce the number of free matrix elements in the viscosity tensor. In particular, in 2D we have 3 independent elements that can be represented by a symmetric rank-2 tensor

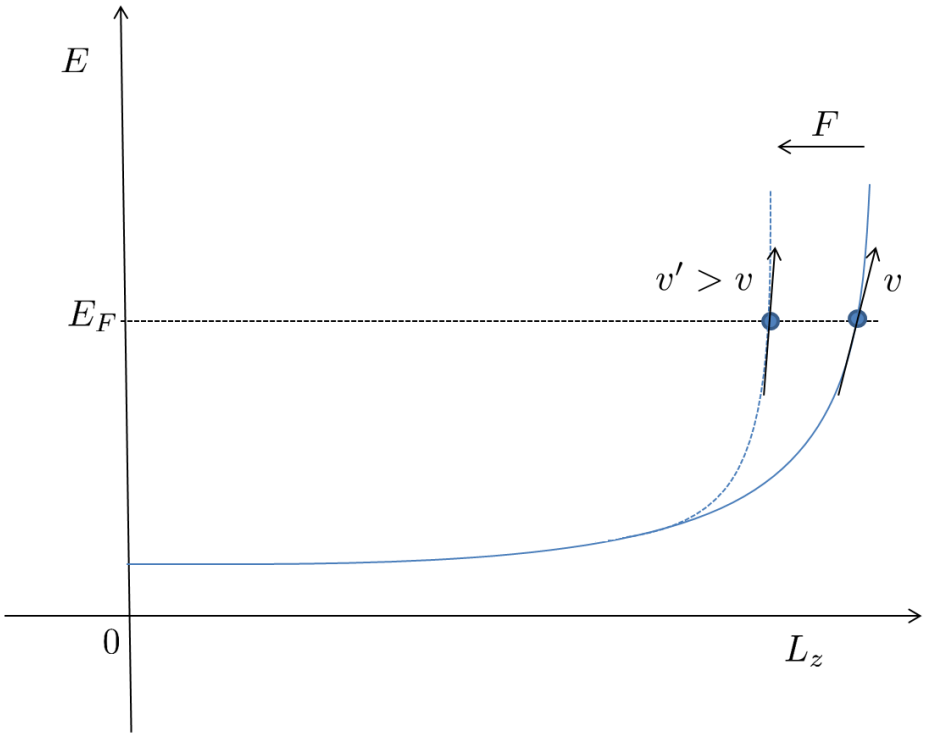

Figure 4.4: Sketch of a quantum Hall droplet under a external force on the edge that tries to compress the system. The edge flow velocity increases and absorbs the force while the interior feels no impact.

η^H_{ab}. This is shown as

$$\eta^{e\,f}_{b\,d} = \epsilon^{ae}\epsilon^{cf}\eta^H_{abcd}, \tag{4.6}$$

$$\begin{aligned}\eta^H_{abcd} &= \eta^H_{bacd} = \eta^H_{abdc} = -\eta^H_{cdab} \\ &= \tfrac{1}{2}\epsilon\left(\epsilon_{ac}\eta^H_{bd} + \epsilon_{ad}\eta^H_{bc} + \epsilon_{bc}\eta^H_{ad} + \epsilon_{bd}\eta^H_{ac}\right),\end{aligned} \tag{4.7}$$

where $\epsilon \equiv \epsilon_{12}$ is the Pfaffian of the 2D Levi-Civita symbol. The tensor η^H_{ab} is odd under time-reversal and will be called the 2D Hall viscosity tensor.

The 2D Hall viscosity tensor was first calculated for the IQHE by Avron, Seiler and Zograf[3]. Later Read[36] generalized the calculation to include the FQHE assuming

rotational symmetry. There η^H_{ab} is proportional to the Euclidean metric

$$\eta^H_{ab} = \eta^H \delta_{ab}, \tag{4.8}$$

with the scalar η^H interpreted as the density of "intrinsic orbital angular momentum"

$$\eta^H = \tfrac{1}{2}\hbar n_e \bar{s}, \tag{4.9}$$

where $n_e = \nu/2\pi l_B^2$ is the electron density and $\bar{s}$ is the average orbital angular momentum. For the IQHE, the orbital angular momentum for the nth Landau level is numerically equal to the topological spin $s_n = n + \frac{1}{2}$ defined in the previous chapter, and this coincidence led to an identification in the literature between the scalar Hall viscosity and the shift. However, the two quantities have completely different origins. We elaborated on the topological nature of the shift (or the topological spin) in Sec.(3.3) while the concept of "angular momentum" depends on the presence of rotational symmetry. In a generic setting, these two quantities should have no relations. In the next section we will derive a generic formula for the 2D Hall viscosity tensor, which is, perhaps not surprisingly, proportional to the natural metric specific to each Landau level.

4.3 2D Hall viscosity tensor

Let's revisit the definition of the stress tensor. In a variational approach, the stress tensor is defined through the variation of an action under an infinitesimal diffeomorphism of the matter fields $\varphi(x) \mapsto \varphi(x') = \varphi(x + \delta u(x))$,

$$\delta S = \int d^4x \sqrt{(-g)} T^\mu_{\ \nu} \nabla_\mu \delta u^\nu, \tag{4.10}$$

where ∇_a is the covariant derivative associated with the metric $g_{\mu\nu}$ and $\sqrt{(-g)}$ is the square root of the determinant of $g_{\mu\nu}$. In field theory the stress tensor is also defined as the variation against a change in the inverse metric

$$\delta S = -\tfrac{1}{2}\int d^4x\sqrt{(-g)}T_{\mu\nu}\delta g^{\mu\nu}. \tag{4.11}$$

However, it is clear that the two definitions give two tensors of different index placement. We argued in Sec.(4.1) that the stress tensor should be a (1,1) tensor, so the first definition is fundamental. Then what is wrong with the second definition? Actually it assumes there is a Lorentz symmetry so that

$$g_{\mu\sigma}T^{\sigma}_{\ \nu} - T^{\sigma}_{\ \mu}g_{\sigma\nu} = 0, \tag{4.12}$$

i.e., the tensor $T_{\mu\nu} \equiv g_{\mu\sigma}T^{\sigma}_{\ \nu}$ is symmetric, which is implicit in the second definition. Notice that the change in the inverse metric under the diffeomorphism is

$$\delta g^{\mu\nu} = -(g^{\mu\sigma}\nabla_\sigma \delta u^\nu + g^{\nu\sigma}\nabla_\sigma \delta u^\mu), \tag{4.13}$$

with which we can show that the two definition are equivalent when Eq.(4.12) is valid.

To explicitly calculate the stress tensor for a generic Hamiltonian, we will use the fundamental definition in Eq.(4.10) for an action describing a 2DEG in $U(1)$ gauge fields A_0 and A_a

$$S = \int d^2x dt\, \mathcal{L}, \tag{4.14}$$

$$\mathcal{L} = \frac{i}{2}\hbar\psi^\dagger\partial_0\psi - \frac{i}{2}\hbar(\partial_0\psi^\dagger)\psi + eA_0\psi^\dagger\psi - \mathcal{H}, \tag{4.15}$$

where the fermionic fields obey the algebra

$$\{\psi(\boldsymbol{x}), \psi(\boldsymbol{x}')\} = \{\psi^\dagger(\boldsymbol{x}), \psi^\dagger(\boldsymbol{x}')\} = 0, \tag{4.16}$$

$$\{\psi(\boldsymbol{x}), \psi^\dagger(\boldsymbol{x}')\} = i\delta^{(2)}(\boldsymbol{x} - \boldsymbol{x}'). \tag{4.17}$$

We have assumed that the underlying manifold is the 2D Euclidean plane, *i.e.*, $g_{ab} = \delta_{ab}$ and $\sqrt{g} = 1$. The Hamiltonian density $\mathcal{H}$ is just the generic form (2.30) written in the field theoretic language. For example, for a system with Galilean invariance it is just

$$\mathcal{H} = \frac{1}{2} m^{ab} (D_a \psi)^\dagger D_b \psi, \tag{4.18}$$

$$D_a = \hbar \partial_a - ieA_a. \tag{4.19}$$

Under an infinitesimal spatial diffeomorphism $x'^a = x^a + \delta u^a$ the $U(1)$-covariant derivatives transform as

$$D'_a = (\delta^b_a - \partial_a \delta u^b) D_b, \tag{4.20}$$

and the variation of the action is

$$\delta S = \int d^2x dt \, T^a_{\ b} \partial_a \delta u^b, \tag{4.21}$$

$$T^a_{\ b} = \frac{\delta \mathcal{H}}{\delta (D_a \psi)^\dagger} (D_b \psi)^\dagger + \frac{\delta \mathcal{H}}{\delta (D_a \psi)} D_b \psi + \mathcal{L} \delta^a_b. \tag{4.22}$$

For the IQHE, which is essentially a single-particle problem, the stress tensor can be written in terms of single-particle operators by tracing out the guiding-center part

$$\mathrm{Tr}(e^{i\boldsymbol{q}\cdot\boldsymbol{R}}) = 2\pi \delta^2(\boldsymbol{q}\ell_B). \tag{4.23}$$

The result is then (the $\mathcal{L}\delta^a_b$ term is identically zero and dropped)

$$T^a_{\ b} = \frac{1}{2\pi l_B^2}\tau^a_{\ b}, \tag{4.24}$$

$$\tau^a_{\ b} = \frac{1}{2}\{v^a, p_b\}, \quad v^a = \frac{\partial H(\boldsymbol{p})}{\partial p_a} = i(\hbar eB)^{-1}\epsilon^{ab}[p_b, H], \tag{4.25}$$

where $H(\boldsymbol{p})$ is the single-particle Hamiltonian. The traceless part of the stress tensor can also be obtained

$$\tilde{\tau}^a_{\ b} = \tau^a_{\ b} - \tfrac{1}{2}\tau^c_{\ c}\delta^a_{\ b} = -i\epsilon^{ac}[\gamma_{bc}, H(\boldsymbol{p})], \tag{4.26}$$

where the γ_{ab} operators are defined in Eq.(2.19).

Now we are ready to calculate the response of the stress tensor to a spatially-uniform time-varying shear strain $\partial_a \delta u^b(t) \equiv \lambda^b_{\ a}(t)$. The perturbative Hamiltonian is

$$\delta\varepsilon(t) = -\tau^a_{\ b}\lambda^b_{\ a}(t) = -\tilde{\tau}^a_{\ b}\lambda^b_{\ a}(t), \tag{4.27}$$

where we have used the fact that $\lambda^a_{\ a}(t) = 0$ (shear strain). According to linear response theory, the induced stress is determined by the retarded stress-stress correlation function,

$$\tilde{\tau}^a_{\ b}(t) = \int dt' G^{a\ c}_{\ b\ d}(t-t')\lambda^d_{\ c}(t'), \tag{4.28}$$

$$G^{a\ c}_{\ b\ d}(t) = \sum_n \frac{\nu_n}{\hbar} i\Theta(t)\langle\Psi_n|[\tilde{\tau}^a_{\ b}(t), \tilde{\tau}^c_{\ d}(0)]|\Psi_n\rangle, \tag{4.29}$$

where $\Theta(t)$ is the step function ($\Theta(t) = 1$ for $t \geq 0$ and $\Theta(t) = 0$ for $t < 0$), $\nu_n = 0$ or 1 is the filling factor for the nth Landau level and Ψ_n are the eigenstates of H. We

then Fourier-transform it into frequency space,

$$G^{a\ c}_{\ b\ d}(\omega) = \int dt\, e^{i(\omega+i\eta)t} G^{a\ c}_{\ b\ d}(t), \tag{4.30}$$

where η is an infinitesimal positive number. The Hall viscosity is the response to the time derivative of the strain, which corresponds to the first order term in the ω-expansion,

$$\begin{aligned}\left.\frac{dG^{a\ c}_{\ b\ d}(\omega)}{d\omega}\right|_{\omega=0} &= \sum_{n,n'} \frac{\hbar\nu_n}{(E_n - E_{n'})^2} \left(\langle n|\tilde{\tau}^a_b|n'\rangle\langle n'|\tilde{\tau}^c_d|n\rangle - \langle n|\tilde{\tau}^c_d|n'\rangle\langle n'|\tilde{\tau}^a_b|n\rangle\right) \\ &= \sum_n \hbar\nu_n \epsilon^{ae}\epsilon^{cf}\langle n|[\gamma_{be},\gamma_{df}]|n\rangle. \end{aligned} \tag{4.31}$$

where E_n are the Landau level energies and we simplified our notation by $|\Psi_n\rangle \equiv |n\rangle$. Comparing it to the definition of the viscosity (4.1), we arrive at the expression for the rank-4 tensor

$$\eta^H_{abcd} = -\frac{i\hbar}{2\pi l_B^2}\sum_n \nu_n \langle n|[\gamma_{bc},\gamma_{de}]|n\rangle. \tag{4.32}$$

Recall the commutator of the γ_{ab} operators in Eq.(2.20), and we obtain the expression for the 2D Hall viscosity tensor

$$\eta^H_{ab} = \frac{\hbar}{2\pi l_B^2}\sum_n \nu_n \langle n|\gamma_{ab}|n\rangle. \tag{4.33}$$

We see that the contribution from each Landau level is proportional to its own natural metric describing the shape of the orbits in that level. The natural metric has nothing to do with the topological spin (although we used the natural metric to construct coherent states that allowed us to define the topological spin). Only when rotational

symmetry is restored, all Landau levels have the same metric and

$$\eta^H_{ab} = \frac{\hbar}{2}\frac{1}{2\pi l_B^2}\left(\sum_n \nu_n s_n\right)\delta_{ab}, \tag{4.34}$$

where $s_n = n + \frac{1}{2}$ is numerically equal to the topological spin.

The generic formula has a property that it is diagonal with respect to the Landau level index and doesn't depend on inter-Landau-level mixing. In the next chapter where we calculate electromagnetic responses, we will differentiate between universal terms that are diagonal and non-universal terms that depend on inter-Landau-level mixing.

4.4 Dipole on the edge

In the last section we showed that the generic Hall viscosity should not be identified with the topological spin. However it does have a relation with a property on the edge. Haldane[18] first pointed out that the Hall viscosity, a quantity defined in the bulk, is related to the intrinsic dipole moment on the edge. This is a manifestation of the bulk-edge correspondence.

To understand this relation, note that there is a discontinuity of the Hall viscosity on the boundary. This discontinuity leaves a net stress force on the boundary, which, for the boundary to remain static, must be balanced by a force from the electric field gradient (that induces the velocity gradient) on an intrinsic electric dipole moment dp^a. Let dL^a be an infinitesimal line segment on the boundary, then

$$T^b_{\ a} dL^b = \eta^{a\ c}_{\ b\ d}\nabla_c v^d dL^b = -dp^b \nabla_b E_a. \tag{4.35}$$

Using

$$v^a = \frac{\epsilon^{ab} E_b}{B}, \tag{4.36}$$

we have

$$dp^a = B^{-1} \epsilon^{ab} \eta^H_{bc} dL^c. \tag{4.37}$$

This correspondence allows a calculation of η^H_{bc} from the edge dipole[34]. For the IQHE, the dipole on the edge is related to the shape of the Gaussian tail and this is consistent with our generic result Eq.(4.33) where η^H_{bc} is proportional to the natural metric that describes the shape of the Landau orbits. For the FQHE, apart from the dipole of the Gaussian tail, there is another contribution coming from the dipole of orbital occupation number. Fig.(4.4) gives the profile of occupation number for Laughlin 1/3 state. Toward the edge the occupation number rises to a peak and then drops steeply. This behavior is due to the squeezing property of the model wavefunction mentioned in Sec.(1.2).

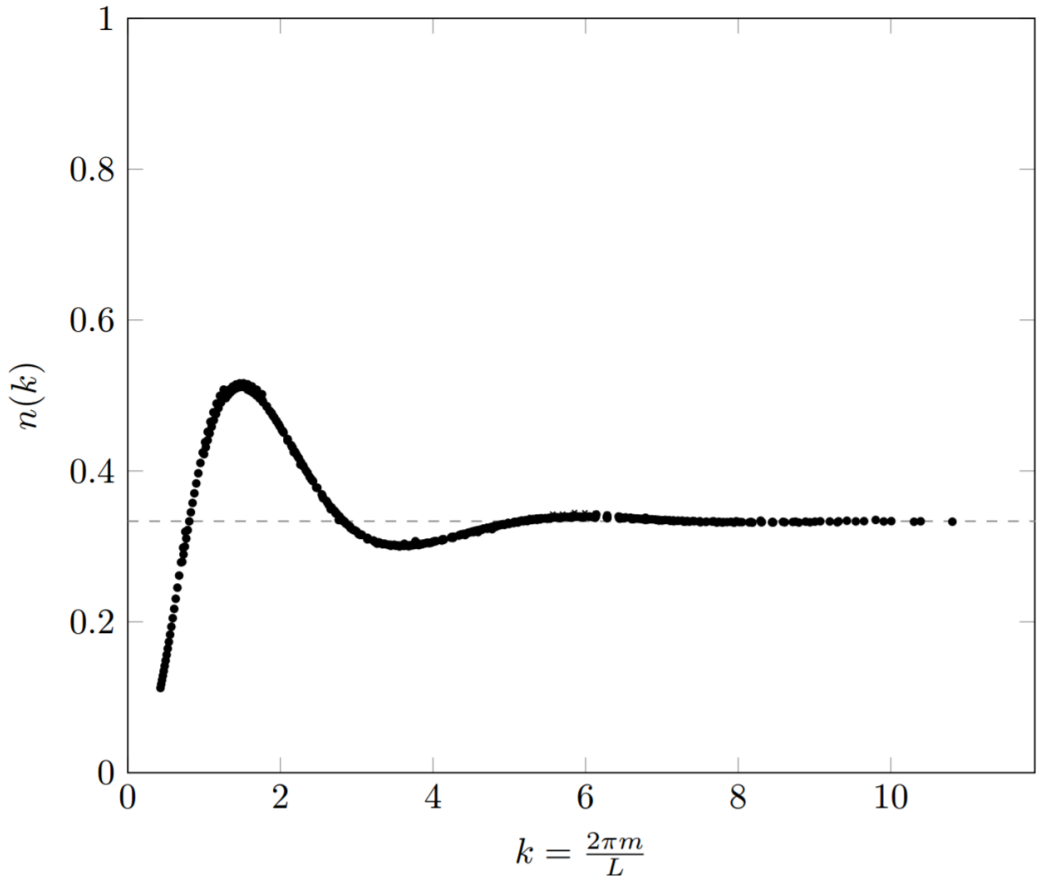

Figure 4.5: Occupation number $n(k)$ for 15 electrons in Lauglin 1/3 state on a cylinder with varying circumferences L from 12.5 to 22 with an increment of 0.5. The dashed line is the average 1/3.[34]

Chapter 5

Electromagnetic responses

In this chapter we will discuss the electromagnetic responses of particle- and current-density without Galilean or rotational symmetry. We will add ingredients to the Heisenberg algebra that will come in handy in our calculation. Particularly, a formal expansion for the current-density operator in momentum space is provided. Then the generic response functions will be derived and compared with previous results in the literature. The identification due to Galilean invariance between the 2D Hall viscosity and the q^2 term in the Hall conductivity will be shown to break down in the generic case and our approach uncovers hidden geometrical properties in the IQHE.

5.1 Heisenberg algebra

In the previous chapters we have made use of the Heisenberg algebra $\mathfrak{h}_2$ of the momentum operators whose commutator is a c-number. The universal enveloping algebra $\mathbb{U}(\mathfrak{h}_2)$ is spanned by the basis

$$\{1, p_a, \{p_a, p_b\}, \{p_a, p_b, p_c\}, \dots\} \tag{5.1}$$

where $\{A, B, \ldots, C\}$ is the symmetrized product of n operators normalized so that $\{\lambda A, \lambda A, \ldots, \lambda A\} = n!(\lambda A)^n$. The single-particle Hamiltonian is built on $\mathbb{U}(\mathfrak{h}_2)$. The Hamiltonian in this chapter will be in its most generic form

$$h = H(\boldsymbol{p}) \equiv \sum_n \frac{1}{n!} H_n^{a_1, a_2, \ldots a_n} p_{a_1} p_{a_2} \ldots p_{a_n} \tag{5.2}$$

where the coefficients $H_n^{a_1 \ldots a_n}$ are fully symmetric in all indices.

When deriving the Hall viscosity formula we used the derivative of the Hamiltonian with the momentum components. Here we will define the derivative in a more formal way using the unitary boost operator parametrized by a real c-number vector $\boldsymbol{q}$

$$U(\boldsymbol{q}) = U(-\boldsymbol{q})^\dagger = e^{i\boldsymbol{q}\cdot\tilde{\boldsymbol{R}}}, \quad [q_a, q_b] = 0. \tag{5.3}$$

Then

$$U(-\boldsymbol{q})\boldsymbol{p}U(\boldsymbol{q}) = \boldsymbol{p} + \hbar\boldsymbol{q}. \tag{5.4}$$

and the derivatives $h^{a_1 a_2 \ldots a_n}$ of h are defined by

$$h(\boldsymbol{q}) \equiv U(-\boldsymbol{q})hU(\boldsymbol{q}) = \sum_{n=0}^{\infty} \frac{\hbar^n}{n!} h^{a_1 a_2 \ldots a_n} q_{a_1} q_{a_2} \ldots q_{a_n}, \tag{5.5}$$

where the tensor-valued operators $h^{a_1 a_2 \ldots a_n}$ are fully symmetric in their indices. In particular, the first derivative h^a is the velocity operator v^a. Note also that

$$U(-\boldsymbol{q})U(-\boldsymbol{q}')\boldsymbol{p}U(\boldsymbol{q}')U(\boldsymbol{q}) = U(-(\boldsymbol{q}+\boldsymbol{q}'))\boldsymbol{p}U(\boldsymbol{q}+\boldsymbol{q}'). \tag{5.6}$$

From this

$$U(-\boldsymbol{q})h^{a_1, \ldots a_m}U(\boldsymbol{q}) = \sum_{n=0}^{\infty} \frac{\hbar^n}{n!} h^{a_1 \ldots a_m b_1 \ldots b_n} q_{b_1} \ldots q_{b_n}. \tag{5.7}$$

as in the differentiation of c-number functions, where $(f')' = f''$.

Now let $\boldsymbol{a} \in \mathbb{U}(\mathfrak{h})$ be a vector-valued operator and λ be a c-number. Then define the expansion

$$H(\boldsymbol{p} + \lambda \boldsymbol{a}) = h + \lambda h_1(\boldsymbol{a}) + O(\lambda^2). \tag{5.8}$$

The quantity $h_1(\boldsymbol{a})$ can be expressed in two equivalent ways as the nested-commutator expansions

$$\begin{aligned} h_1(\boldsymbol{a}) &= a_{a_1} h^{a_1} + \frac{1}{2!}[p_{a_1}, a_{a_2}] h^{a_1 a_2} + \frac{1}{3!}[p_{a_1}, [p_{a_2}, a_{a_3}]] h^{a_1 a_2 a_3} + \ldots & (5.9) \\ &= h^{a_1} a_{a_1} + \frac{1}{2!} h^{a_1 a_2}[a_{a_1}, p_{a_2}] + \frac{1}{3!} h^{a_1 a_2 a_3}[[a_{a_1}, p_{a_2}], p_{a_3}] + \ldots . & (5.10) \end{aligned}$$

This will be useful when we introduce perturbation to the gauge fields and thus to the momentum operators.

The operator h is also a function of the scale factor B_0, the constant magnetic field, and more properly should be written as $h(B_0)$. The magnetization operator $m(\boldsymbol{p})$ is defined by

$$\begin{aligned} m &\equiv -\left.\frac{\partial h}{\partial B_0}\right|_{\{H_n\}} = -\tfrac{1}{2} B_0^{-1} h_1(\boldsymbol{p}) \\ &= -\tfrac{1}{2} B_0^{-1} \boldsymbol{v} \cdot \boldsymbol{p} = -\tfrac{1}{2} B_0^{-1} \boldsymbol{p} \cdot \boldsymbol{v} = \tfrac{1}{2} B_0^{-1} \left(h + i\ell_B^{-2} \epsilon_{ab} \tilde{R}^a h \tilde{R}^b \right). \end{aligned} \tag{5.11}$$

If the Hamiltonian is a quadratic operator, $h = \frac{1}{2} H_2^{ab} p_a p_b$, then $B_0 m = -h$, i.e. the shape of the Landau orbits is independent of the scaling of the magnetic field. This is also true for a rotationally invariant Hamiltonian. Actually for any scalar operator $O \in \mathbb{U}(\mathfrak{h}_2)$, one can define the scale derivative

$$dO \equiv B_0 \frac{\partial O}{\partial B_0} = \tfrac{1}{2} \left(-i\ell_B^{-2} \epsilon_{ab} \tilde{R}^a O \tilde{R}^b - O \right), \tag{5.12}$$

and by definition

$$dh = -B_0 m. \tag{5.13}$$

Higher orders of derivatives can be recursively defined as

$$d^{n+1}O \equiv B_0 \frac{\partial(d^n O)}{\partial B_0}, \quad d^1 O \equiv dO. \tag{5.14}$$

Note that if $Q \equiv \boldsymbol{q} \cdot \tilde{\boldsymbol{R}} \in \mathfrak{h}$, then

$$QO\tilde{R}^a - \tilde{R}^a OQ = [Q, R^a](O + 2dO) \tag{5.15}$$

where $[Q, R^a]$ is a c-number,

For IQHE, the only formula we need for the guiding-center part is

$$\mathrm{Tr}(e^{i\boldsymbol{q}\cdot\boldsymbol{R}}) = 2\pi\delta^2(\boldsymbol{q}\ell_B) \tag{5.16}$$

where the trace is over the Hilbert space of the guiding-center, and $\delta^2(\boldsymbol{x})$ is the 2D Dirac delta-function.

5.2 Current density operator

In this section we will derive an expansion of the current-density operator to all orders in $\boldsymbol{q}$. Introduce an additional vector potential

$$A_a(\boldsymbol{x}) = \int \frac{d^2\boldsymbol{q}}{(2\pi)^2} \tilde{A}_a(\boldsymbol{q}) e^{i\boldsymbol{q}\cdot\boldsymbol{x}}, \tag{5.17}$$

with

$$\delta B(\boldsymbol{x}) = \partial_1 A_2(\boldsymbol{x}) - \partial_2 A_1(\boldsymbol{x}), \tag{5.18}$$

and define the operator

$$A_a \equiv \int \frac{d^2\boldsymbol{q}}{(2\pi)^2} \tilde{A}_a(\boldsymbol{q}) e^{i\boldsymbol{q}\cdot\boldsymbol{R}} U(\boldsymbol{q}). \tag{5.19}$$

The problem of the charged particle moving in the 2D plane $\boldsymbol{x}$ in the presence of a non-uniform magnetic flux density $B_0 + \delta B(x)$ is then described by the Hamiltonian

$$H = H(\boldsymbol{p} - e\boldsymbol{A}). \tag{5.20}$$

The electric charge density operator is given by

$$J^0(\boldsymbol{x}) = e \int \frac{d^2\boldsymbol{q}}{(2\pi)^2} e^{i\boldsymbol{q}(\boldsymbol{R}-\boldsymbol{x})} U(\boldsymbol{q}), \tag{5.21}$$

and the electric current-density operator is given by

$$J^a(\boldsymbol{x}) = e \int \frac{d^2\boldsymbol{q}}{(2\pi)^2} e^{i\boldsymbol{q}\cdot(\boldsymbol{R}-\boldsymbol{x})} J^a(\boldsymbol{q}). \tag{5.22}$$

To find the expression for $J^a(\boldsymbol{q})$, notice the continuity equation (gauge invariance) requires

$$(i\hbar)^{-1}[J^0(\boldsymbol{x}), h] + \partial_a J^a(\boldsymbol{x}) = 0, \tag{5.23}$$

or in the $\boldsymbol{q}$ space

$$[h, U(\boldsymbol{q})] = \hbar q_a J^a(\boldsymbol{q}). \tag{5.24}$$

Then the functional form of the expansion of $J^a(\boldsymbol{q})$ must be

$$\hbar J^a(\boldsymbol{q}) = -i[\alpha^a(\boldsymbol{q}), h] + i\epsilon^{ba} q_b \ell_B^2 \beta(\boldsymbol{q}). \tag{5.25}$$

where

$$iq_a \alpha^a(\boldsymbol{q}) = U(\boldsymbol{q}) - 1 \tag{5.26}$$

or

$$\alpha^a(\boldsymbol{q}) = -i\frac{\partial}{\partial q_a}\left(\sum_{n=1}^{\infty} \frac{1}{n} \frac{(i\boldsymbol{q}\cdot\tilde{\boldsymbol{R}})^n}{n!}\right) = \sum_{n=1}^{\infty} \frac{1}{n}\frac{1}{n!} \sum_{k=1}^{n} (iQ)^{k-1} \tilde{R}^a (iQ)^{n-k}. \tag{5.27}$$

This must be satisfied at each order of an expansion in $\tilde{A}_a(\boldsymbol{q})$ and to leading order

$$e_a J^a(\boldsymbol{q}) = h_1(\boldsymbol{e}U(\boldsymbol{q})) + O(\tilde{\boldsymbol{A}}), \tag{5.28}$$

where $\boldsymbol{e}$ is a c-number unit vector. In this section we focus on the first term $h_1(\boldsymbol{e}U(\boldsymbol{q}))$. Using (5.9) the explicit form of $J^a(\boldsymbol{q})$ can be written as

$$i\hbar J^a = U(\boldsymbol{q})\left([\tilde{R}^a, h] + \frac{1}{2!}[-iQ, [\tilde{R}^a, h]] + \frac{1}{3!}[-iQ, [-iQ, [\tilde{R}^a, h]]] + \cdots\right), \tag{5.29}$$

where $Q = \boldsymbol{q}\cdot\tilde{\boldsymbol{R}}$ as mentioned above. Expanding $U(\boldsymbol{q})$ and the nested commutators gives

$$i\hbar J^a = \sum_{m=0}^{\infty}\frac{(iQ)^m}{m!}\sum_{n=0}^{\infty}(-1)^n\frac{1}{(n+1)!}\sum_{k=0}^{n}(-1)^k\binom{n}{k}(iQ)^{n-k}[\tilde{R}^a, h](iQ)^k. \tag{5.30}$$

Recollect the terms in the form of

$$(iQ)^l[\tilde{R}^a, h](iQ)^k$$

and the corresponding coefficient $C_{l,k}$ is (using $l+k = m+n$)

$$\begin{aligned} C_{l,k} &= \sum_{m=0}^{l}\frac{1}{m!}(-1)^{l+k-m}\frac{1}{(l+k-m+1)!}(-1)^k\binom{l+k-m}{k} \\ &= \frac{1}{k!l!}\sum_{m=0}^{l}(-1)^m\frac{1}{k+m+1}\binom{l}{m} \\ &= \frac{1}{(k+l+1)!}. \end{aligned} \tag{5.31}$$

Now a significantly simplified form for $J^a(\boldsymbol{q})$ can be written down

$$i\hbar J^a = \sum_{n=0}^{\infty}\frac{1}{(n+1)!}\sum_{k=0}^{n}(iQ)^{n-k}[\tilde{R}^a, h](iQ)^k, \tag{5.32}$$

which is further reduced into the desired form:

$$
\begin{aligned}
i\hbar J^a =& \sum_{n=0}^{\infty} \frac{1}{(n+1)!} \left((iQ)^n \tilde{R}^a h - h\tilde{R}^a (iQ)^n - i \sum_{k=0}^{n-1} (iQ)^{n-1-k} (Qh\tilde{R}^a - \tilde{R}^a hQ)(iQ)^k \right) \\
=& \sum_{n=0}^{\infty} \frac{1}{(n+1)!} \left(\frac{1}{2}\{(iQ)^n, \tilde{R}^a\}h + \frac{1}{2}[(iQ)^n, \tilde{R}^a]h - \frac{1}{2}h\{\tilde{R}^a, (iQ)^n\} + \frac{1}{2}h[(iQ)^n, \tilde{R}^a] \right. \\
& \left. -i[Q, \tilde{R}^a] \sum_{k=0}^{n-1} (iQ)^{n-1-k} (h + 2dh)(iQ)^k \right) \\
=& \sum_{n=0}^{\infty} \frac{1}{(n+1)!} \left(\left[\frac{1}{2}\{(iQ)^n, \tilde{R}^a\}, h \right] - i[Q, \tilde{R}^a] \sum_{k=0}^{n-1} (iQ)^{n-1-k} (2dh)(iQ)^k \right. \\
& \left. +i[Q, \tilde{R}^a] \left(\frac{n}{2}(iQ)^{n-1}h + \frac{n}{2}h(iQ)^{n-1} - \sum_{k=0}^{n-1} (iQ)^{n-1-k} h (iQ)^k \right) \right) \\
=& [\alpha^a(\boldsymbol{q}), h] + i[Q, \tilde{R}^a]\beta(\boldsymbol{q})
\end{aligned}
\tag{5.33}
$$

where

$$
\alpha^a(\boldsymbol{q}) = \sum_{n=0}^{\infty} \frac{1}{2(n+1)!} \{(iQ)^n, \tilde{R}^a\}, \tag{5.34}
$$

$$
\beta(\boldsymbol{q}) = -\sum_{n=0}^{\infty} \frac{2}{(n+1)!} \sum_{k=0}^{n-1} (iQ)^{n-1-k} (dh)(iQ)^k + \sum_{n=0}^{\infty} \frac{1}{2(n+1)!} \sum_{k=0}^{n-1} [(iQ)^{n-1-k}, [(iQ)^k, h]]. \tag{5.35}
$$

The expansion for $\alpha^a(\boldsymbol{q})$ agrees with the universal form (5.27), and the leading term in $\beta(\boldsymbol{q})$ is just $-dh = B_0 m$.

5.3 Response functions

We are ready to calculate the responses for a non-uniform magnetic field and a non-zero electric field. The perturbed Hamiltonian is

$$H = h - e\int \frac{d^2\boldsymbol{q}}{(2\pi)^2}\tilde{A}_0(\boldsymbol{q})U(\boldsymbol{q})e^{i\boldsymbol{q}\cdot\boldsymbol{R}} - e\int \frac{d^2\boldsymbol{q}}{(2\pi)^2}\tilde{A}_a(\boldsymbol{q})J^a(\boldsymbol{q})e^{i\boldsymbol{q}\cdot\boldsymbol{R}} - e^2\int \frac{d^2\boldsymbol{q}}{(2\pi)^2}\tilde{A}_a(-\boldsymbol{q})\Gamma^{ab}(\boldsymbol{q})\tilde{A}_b(\boldsymbol{q})e^{i\boldsymbol{q}\cdot\boldsymbol{R}} + \mathcal{O}(\tilde{A}_a^3), \tag{5.36}$$

where $\Gamma^{ab}(\boldsymbol{q})$ is a gauge counter-term that is important for ensuring gauge invariance. It gives the $O(\tilde{\boldsymbol{A}})$ dependence of the complete current-density operator. Its explicit form is:

$$\begin{aligned}\Gamma^{ab}(\boldsymbol{q}) =& \frac{1}{\hbar^2}\sum_{n=0}^{\infty}\frac{1}{(n+2)!}[\overbrace{iQ,\cdots[iQ}^{\text{n}},[\tilde{R}^a,[h,\tilde{R}^b]]]\cdots] \\ &+ \frac{1}{\hbar^2}\sum_{n=0}^{\infty}\frac{1}{(n+2)!}[\overbrace{-iQ,\cdots[-iQ}^{\text{n}},[\tilde{R}^a,[h,\tilde{R}^b]]]\cdots] \\ =& \frac{1}{\hbar^2}\sum_{k=0}^{\infty}\frac{2}{(2k+2)!}[\overbrace{iQ,\cdots[iQ}^{\text{n}},[\tilde{R}^a,[h,\tilde{R}^b]]]\cdots].\end{aligned} \tag{5.37}$$

The perturbed particle density and current density in the nth Landau level are

$$\delta J_n^0(\boldsymbol{x}) = -\frac{e}{2\pi\ell_B^2}\left(\int \frac{d^2\boldsymbol{q}}{(2\pi)^2}\chi_n^{00}(\boldsymbol{q})\tilde{U}(\boldsymbol{q})e^{i\boldsymbol{q}\cdot\boldsymbol{x}} + \int \frac{d^2\boldsymbol{q}}{(2\pi)^2}\chi_n^{0a}(\boldsymbol{q})\tilde{A}_q(\boldsymbol{q})e^{i\boldsymbol{q}\cdot\boldsymbol{x}}\right), \tag{5.38}$$

$$\delta J_n^a(\boldsymbol{x}) = -\frac{e}{2\pi\ell_B^2}\left(\int \frac{d^2\boldsymbol{q}}{(2\pi)^2}\chi_n^{0a}(-\boldsymbol{q})\tilde{A}_0(\boldsymbol{q})e^{i\boldsymbol{q}\cdot\boldsymbol{x}} + \int \frac{d^2\boldsymbol{q}}{(2\pi)^2}\tilde{\chi}_n^{ab}(\boldsymbol{q})\tilde{A}_b(\boldsymbol{q})e^{i\boldsymbol{q}\cdot\boldsymbol{x}}\right), \tag{5.39}$$

where the correlation functions are density-density

$$\chi_n^{00}(\boldsymbol{q}) = \sum_{n'(\neq n)}\frac{\langle n|U(-\boldsymbol{q})|n'\rangle\langle n'|U^a(\boldsymbol{q})|n\rangle + \langle n|U(\boldsymbol{q})|n'\rangle\langle n'|U(-\boldsymbol{q})|n\rangle}{E_n - E_{n'}}, \tag{5.40}$$

density-current

$$\chi_n^{0a}(\boldsymbol{q}) = \sum_{n'(\neq n)} \frac{\langle n|U(-\boldsymbol{q})|n'\rangle\langle n'|J^a(\boldsymbol{q})|n\rangle + \langle n|J^a(\boldsymbol{q})|n'\rangle\langle n'|U(-\boldsymbol{q})|n\rangle}{E_n - E_{n'}}, \tag{5.41}$$

current-current

$$\chi_n^{ab}(\boldsymbol{q}) = \sum_{n'(\neq n)} \frac{\langle n|J^a(-\boldsymbol{q})|n'\rangle\langle n'|J^b(\boldsymbol{q})|n\rangle + \langle n|J^b(\boldsymbol{q})|n'\rangle\langle n'|J^a(-\boldsymbol{q})|n\rangle}{E_n - E_{n'}}, \tag{5.42}$$

and current-current plus counter-term

$$\tilde{\chi}_n^{ab}(\boldsymbol{q}) = \chi_n^{ab}(\boldsymbol{q}) + \langle n|\Gamma^{ab}(\boldsymbol{q})|n\rangle, \tag{5.43}$$

and E_n and $|n\rangle$ are eigen-energies and eigenstates. Below we will simplify our notation by defining

$$(A, B)_n \equiv \sum_{n'\neq n} \frac{\langle n|A|n'\rangle\langle n'|B|n\rangle + \langle n|B|n'\rangle\langle n'|A|n\rangle}{E_n - E_{n'}}, \tag{5.44}$$

so

$$\chi_n^{00}(\boldsymbol{q}) = (U(-\boldsymbol{q}), U(\boldsymbol{q}))_n, \tag{5.45}$$

$$\chi_n^{0a}(\boldsymbol{q}) = (U(-\boldsymbol{q}), J^a(\boldsymbol{q}))_n, \tag{5.46}$$

$$\chi_n^{ab}(\boldsymbol{q}) = (J^a(-\boldsymbol{q}), J^b(\boldsymbol{q}))_n. \tag{5.47}$$

We will also denote the expectation value of some operator $\mathcal{O}$ in the nth Landau level by $\langle\mathcal{O}\rangle_n$.

Using the expansions of $U(\boldsymbol{q})$ and $J^a(\boldsymbol{q})$, these correlation functions are readily obtained:

$$\chi_n^{00}(\boldsymbol{q}) = -(Q,Q)_n + \mathcal{O}(|\boldsymbol{q}|^4), \tag{5.48}$$

$$\chi_n^{0a}(\boldsymbol{q}) = -\frac{1}{\hbar}[Q,\tilde{R}^a]\left(1 - \frac{1}{6}\langle Q^2\rangle_n + \frac{1}{3}(Q,\{Q,dh\})_n - \frac{1}{2}(Q^2,dh)_n\right) + \mathcal{O}(|\boldsymbol{q}|^5), \tag{5.49}$$

$$\tilde{\chi}_n^{ab}(\boldsymbol{q}) = -\frac{1}{\hbar^2}[Q,\tilde{R}^a][Q,\tilde{R}^b]\left(\langle dh + d^2h\rangle_n + (dh,dh)_n\right) + \mathcal{O}(|\boldsymbol{q}|^4). \tag{5.50}$$

If we define

$$\chi_{E,n}^{ab} = -\frac{e^2}{2\pi l_B^2}(\tilde{R}^a,\tilde{R}^b)_n, \tag{5.51}$$

$$\sigma_n^{ab} = \frac{1}{6}s_n g_n^{ab} - \left[\frac{1}{6}(\tilde{R}^a,\{\tilde{R}^b,dh\})_n + a \leftrightarrow b\right] + \frac{1}{4}(\{\tilde{R}^a,\tilde{R}^b\},dh)_n, \tag{5.52}$$

$$s_n g_n^{ab} = \frac{1}{2}\langle\{\tilde{R}^a,\tilde{R}^b\}\rangle_n, \tag{5.53}$$

$$\chi_{M,n} = \frac{e^2 l_B^2}{2\pi\hbar^2}\left(\langle dh + d^2h\rangle_n + (dh,dh)_n\right), \tag{5.54}$$

then

$$\chi_n^{00}(\boldsymbol{q}) = -\frac{2\pi l_B^2}{e^2}q_a q_b \chi_{E,n}^{ab} + \mathcal{O}(|\boldsymbol{q}|^4), \tag{5.55}$$

$$\chi_n^{0a}(\boldsymbol{q}) = -\frac{1}{\hbar}[Q,\tilde{R}^a]\left(1 - \sigma_n^{ab}q_a q_b\right) + \mathcal{O}(|\boldsymbol{q}|^5), \tag{5.56}$$

$$\tilde{\chi}_n^{ab}(\boldsymbol{q}) = -\frac{2\pi}{e^2 l_B^2}[Q,\tilde{R}^a][Q,\tilde{R}^b]\chi_{M,n} + \mathcal{O}(|\boldsymbol{q}|^4). \tag{5.57}$$

Now using

$$[Q,\tilde{R}^a] = i l_B^2 \epsilon^{ba} q_b, \tag{5.58}$$

$$E(\boldsymbol{q}) = iq\tilde{A}_0(\boldsymbol{q}), \tag{5.59}$$

$$\delta B(\boldsymbol{q}) = i\epsilon^{ab}q_a\tilde{A}_b(\boldsymbol{q}), \tag{5.60}$$

we are able to write down the generic responses (in the absence of rotational symmetry) of particle- and current- density against a non-vanishing electric field and a non-uniform magnetic field:

$$\delta J_n^a = \frac{1}{2\pi l_B^2}\left(1 + \sigma_n^{cd}\partial_c\partial_d\right) v^a - \chi_{M,n}\epsilon^{ab}\partial_b\delta B, \tag{5.61}$$

$$\delta J_n^0 = \frac{1}{2\pi l_B^2}\left(\frac{\delta B}{B_0} + \sigma_n^{ab}\partial_a\partial_b \ln\frac{\delta B}{B_0}\right) - \chi_{E,n}^{ab}\partial_a E_b, \tag{5.62}$$

where the magnetic length l_B is defined with respect to B_0 and $v^a = \epsilon^{ab}E_b/B_0$ is the flow velocity field. Now the physical meaning of the previously defined quantities are obvious: χ_E^{ab} (dropping the Landau level index) is the electric susceptibility tensor that produces a polarization density $P^a = \chi_E^{ab}E_b$, σ^{ab} is the tensor in the q^2 term of the Hall conductivity and $\chi_M(B_0)$ is the magnetic susceptibility at B_0 that produces an extra magnetic moment density $\delta M = \chi_M\delta B$.

5.4 Discussion

We present here again the generic formula for σ^{ab}, the q^2 term of the Hall conductivity,

$$\sigma_n^{ab} = \frac{1}{6}s_n g^{ab} - \left[\frac{1}{6}(\tilde{R}^a, \{\tilde{R}^b, dh\})_n + a \leftrightarrow b\right] + \frac{1}{4}(\{\tilde{R}^a, \tilde{R}^b\}, dh)_n. \tag{5.63}$$

The first term is proportional to the inverse of the 2D Hall viscosity tensor η_{ab}^H. We mentioned in the last chapter that terms being diagonal with respect to the Landau level index are universal as they don't depend on inter-Landau-level mixing. The second and the third terms are inter-Landau-level mixing terms, with the second term between states with opposite parity and the third term the same parity. They depend on the details of the Hamiltonian and are non-universal. When there is rotational symmetry, the third term vanishes because the eigenstates are invariant with respect to rescaling of B_0. When Galilean symmetry is present, the second term

can be explicitly calculated to be

$$-[\frac{1}{6}(\tilde{R}^a,\{\tilde{R}^b,dh\})_n + a \leftrightarrow b] = \frac{4}{3}s_n g^{ab}, \tag{5.64}$$

which combined with the first term gives

$$\sigma_n^{ab} = \frac{3}{2}s_n g^{ab}. \tag{5.65}$$

This agrees with existing results in the literature[1, 38, 24, 5]. However a simple identification of this tensor as the (inverse) 2D Hall viscosity tensor is not valid for a realistic system and thus can not be relied on to measure the Hall viscosity.

The electric susceptibility tensor χ_E^{ab} measures the polarization energy at the presence of a electric field. In a quantum Hall fluid the electric field also induces a flow velocity $v^a = \epsilon^{ab}E_b/B_0$ of the guiding centers. From the perspective of the guiding centers the same energy can be interpreted as the kinetic energy of the guiding centers and the tensor

$$m_{ab} = B_0^2\epsilon_{ac}\epsilon_{bd}\chi_E^{cd} \tag{5.66}$$

acts as the effective mass of the guiding centers. Fig.(5.1) illustrates this idea. Note that this effective mass has nothing to do with the effective mass in a Galilean invariant Hamiltonian that is induced from the band structure.

The magnetic susceptibility χ_M has two terms. The first term is universal and we can write it as

$$\frac{1}{2\pi l_B^2}\langle\frac{2m}{B_0} + \frac{\partial m}{\partial B_0}\rangle_n. \tag{5.67}$$

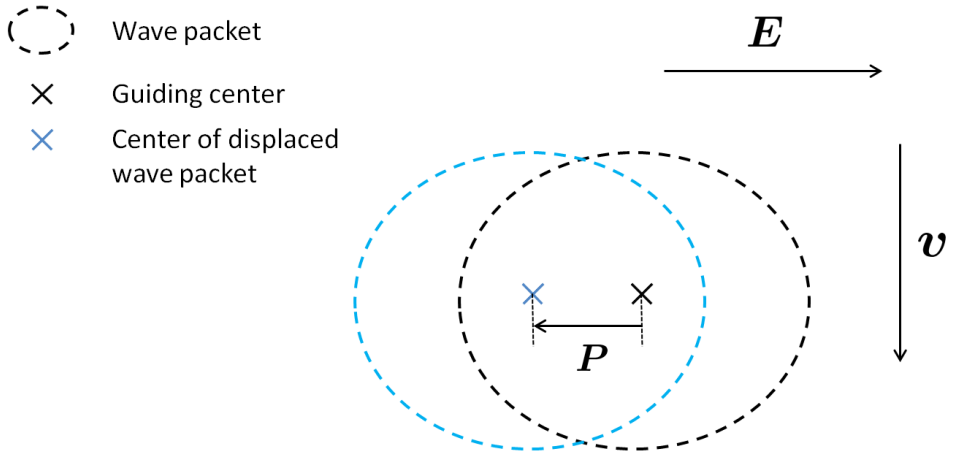

Figure 5.1: Sketch of the formation of a polarization $\boldsymbol{P}$ as the displacement of the center of the wave packet from the original guiding center under an electric field $\boldsymbol{E}$. The guiding center will have a flow velocity determined by $v^a = \epsilon^{ab}E_b/B$. Therefore the induced energy can be considered as either an polarization energy from the Landau-orbit point of view or a kinetic energy from the guiding-center point of view.

The $\partial m/\partial B_0$ part accounts for the change in the magnetization m in the nth Landau level and vanishes for a Galilean system. The second term in χ_M is inter-Landau-level mixing and accounts for the change of the Landau-orbit shape under scaling of the magnetic field when rotational symmetry is absent. Fig.(5.4) summarizes these different cases.

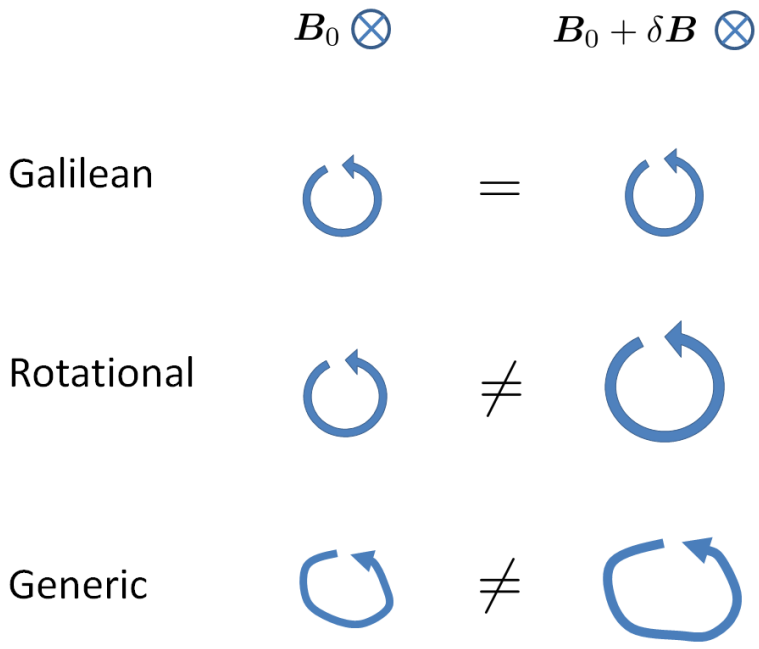

Figure 5.2: Sketch of the magnetization m under a change in the magnetic field. The area enclosed by the loops indicate the magnitude of m and the shape is that of the Landau orbits. For a Galilean invariant system, m doesn't change. For a rotationally invariant system, the change in m originates within a single Landau level and the shape of the Landau orbits doesn't change. In the generic case, the change in m has contributions both from within the Landau level and from inter-Landau-level mixing that also changes the shape of the Landau orbits.

Chapter 6

Conclusion

We presented a generic theory for the IQHE in the absence of Galilean or rotational symmetry. We introduced the algebra of Landau orbits and guiding centers, and used the natural metric of each Landau level to construct guiding-center coherent states. Then we achieved the following three things:

- By numerically solving the eigen problem for a quartic Hamiltonian and investigating the root distribution of the polynomial solutions, we defined the topological spin as the number of central zeros that are enclosed by a fattened version of the semiclassical orbit.

- We calculated the generic formula for the 2D Hall viscosity tensor and found that the contribution from each Landau level is proportional to its natural metric. We also pointed out the identification of the scalar Hall viscosity with the topological spin is only a coincidence at the presence of rotational symmetry.

- We obtained generic electromagnetic responses and clarified the structure of the correlation functions. Particularly the q^2 term of the Hall conductivity was shown to differ from the (inverse) 2D Hall viscosity in the generic case as it contains inter-Landau-mixing terms that are non-universal.

These results have clearly shown that the generic approach is able to:

- differentiate between topological and non-topological quantities;
- reveal richer geometrical properties previously hidden by applying special symmetries.

A possible direction to carry this research further would be a close study on the "gravitational anomaly" term that appears in the effective theory for the QHE[8, 1, 14, 10, 16]. Previous work has treated the metric as that of the underlying manifold. Although the mathematics is well developed in the field theory, that approach doesn't explain much about the physical nature of the term. We believe a truly physical interpretation should be that the metric is a dynamic quantity intrinsic to the system and something that is able to induce a variation in the metric would be either acoustic waves of the underlying crystal lattice or the interactive dynamics of the 2DEG itself. Also Galilean symmetry is not essential to the presence of the term and we would like to see a generic derivation.

It would certainly be wonderful if we could extend this generic approach to the FQHE. In fact, all the concepts used in this thesis have their counterparts in the FQHE and some are indeed mentioned in the discussion. For example, the guiding-center counterpart of the polarization effect in the electromagnetic responses would be due to a shift of the position of the electron away from the center of flux attachment or correlation hole. It is also likely that new concepts, especially geometrical ones, that have no counterparts in the IQHE can emerge in the FQHE when we pursue a generic approach.

Bibliography

[1] Alexander G. Abanov and Andrey Gromov. Electromagnetic and gravitational responses of two-dimensional noninteracting electrons in a background magnetic field. *Phys. Rev. B*, 90:014435, Jul 2014.

[2] Daniel Arovas, J. R. Schrieffer, and Frank Wilczek. Fractional statistics and the quantum hall effect. *Phys. Rev. Lett.*, 53:722–723, Aug 1984.

[3] J. E. Avron, R. Seiler, and P. G. Zograf. Viscosity of quantum hall fluids. *Phys. Rev. Lett.*, 75:697–700, Jul 1995.

[4] B. Andrei Bernevig and F. D. M. Haldane. Model fractional quantum hall states and jack polynomials. *Phys. Rev. Lett.*, 100:246802, Jun 2008.

[5] R. R. Biswas. Semiclassical theory of viscosity in quantum hall states. arXiv:1311.7149, Dec 2013.

[6] Parsa Bonderson, Victor Gurarie, and Chetan Nayak. Plasma analogy and non-abelian statistics for ising-type quantum hall states. *Phys. Rev. B*, 83:075303, Feb 2011.

[7] Barry Bradlyn and N. Read. Low-energy effective theory in the bulk for transport in a topological phase. *Phys. Rev. B*, 91:125303, Mar 2015.

[8] Barry Bradlyn and N. Read. Topological central charge from berry curvature: Gravitational anomalies in trial wave functions for topological phases. *Phys. Rev. B*, 91:165306, Apr 2015.

[9] J. M. Caillol, D. Levesque, J. J. Weis, and J. P. Hansen. A monte carlo study of the classical two-dimensional one-component plasma. *Journal of Statistical Physics*, 28:325–349, June 1982.

[10] T. Can, M. Laskin, and P. Wiegmann. Fractional quantum hall effect in a curved space: Gravitational anomaly and electromagnetic response. *Phys. Rev. Lett.*, 113:046803, Jul 2014.

[11] Gil Young Cho, Yizhi You, and Eduardo Fradkin. Geometry of fractional quantum hall fluids. *Phys. Rev. B*, 90:115139, Sep 2014.

[12] S. M. Girvin. The quantum hall effect: Novel excitations and broken symmetries. arXiv:cond-mat/9907002, July 1999.

[13] S. M. Girvin, A. H. MacDonald, and P. M. Platzman. Magneto-roton theory of collective excitations in the fractional quantum hall effect. *Phys. Rev. B*, 33:2481–2494, Feb 1986.

[14] Andrey Gromov and Alexander G. Abanov. Density-curvature response and gravitational anomaly. *Phys. Rev. Lett.*, 113:266802, Dec 2014.

[15] Andrey Gromov and Alexander G. Abanov. Thermal hall effect and geometry with torsion. *Phys. Rev. Lett.*, 114:016802, Jan 2015.

[16] Andrey Gromov, Gil Young Cho, Yizhi You, Alexander G. Abanov, and Eduardo Fradkin. Framing anomaly in the effective theory of the fractional quantum hall effect. *Phys. Rev. Lett.*, 114:016805, Jan 2015.

[17] F. D. M. Haldane. Fractional quantization of the hall effect: A hierarchy of incompressible quantum fluid states. *Phys. Rev. Lett.*, 51:605–608, Aug 1983.

[18] F. D. M. Haldane. Hall viscosity and intrinsic metric of incompressible fractional hall fluids. arXiv:0906.1854, June 2009.

[19] F. D. M. Haldane. Geometrical description of the fractional quantum hall effect. *Phys. Rev. Lett.*, 107:116801, Sep 2011.

[20] F. D. M. Haldane and E. H. Rezayi. Periodic laughlin-jastrow wave functions for the fractional quantized hall effect. *Phys. Rev. B*, 31:2529–2531, Feb 1985.

[21] F. D. M. Haldane and Y. Shen. Geometry of landau orbits in the absence of rotational symmetry. arXiv:1512.04502v2, May 2016.

[22] B. I. Halperin. Statistics of quasiparticles and the hierarchy of fractional quantized hall states. *Phys. Rev. Lett.*, 52:1583–1586, Apr 1984.

[23] M. Z. Hasan and C. L. Kane. Colloquium. *Rev. Mod. Phys.*, 82:3045–3067, Nov 2010.

[24] Carlos Hoyos and Dam Thanh Son. Hall viscosity and electromagnetic response. *Phys. Rev. Lett.*, 108:066805, Feb 2012.

[25] J. K. Jain. Composite-fermion approach for the fractional quantum hall effect. *Phys. Rev. Lett.*, 63:199–202, Jul 1989.

[26] K. v. Klitzing, G. Dorda, and M. Pepper. New method for high-accuracy determination of the fine-structure constant based on quantized hall resistance. *Phys. Rev. Lett.*, 45:494–497, Aug 1980.

[27] Ilpo Laine. *Nevanlinna Theory and Complex Differential Equations*. Walter de Gruyter, 1993.

[28] R. B. Laughlin. Quantized hall conductivity in two dimensions. *Phys. Rev. B*, 23:5632–5633, May 1981.

[29] R. B. Laughlin. Anomalous quantum hall effect: An incompressible quantum fluid with fractionally charged excitations. *Phys. Rev. Lett.*, 50:1395–1398, May 1983.

[30] Hui Li and F. D. M. Haldane. Entanglement spectrum as a generalization of entanglement entropy: Identification of topological order in non-abelian fractional quantum hall effect states. *Phys. Rev. Lett.*, 101:010504, Jul 2008.

[31] Gregory Moore and Nicholas Read. Nonabelions in the fractional quantum hall effect. *Nuclear Physics B*, 360(23):362 – 396, 1991.

[32] Maho Nakata. The mpack (mblas/mlapack): a multiple precision arithmetic version of blas and lapack, version 0.8.0, 2012, see http://mplapack.sourceforget.net.

[33] Chetan Nayak, Steven H. Simon, Ady Stern, Michael Freedman, and Sankar Das Sarma. Non-abelian anyons and topological quantum computation. *Rev. Mod. Phys.*, 80:1083–1159, Sep 2008.

[34] YeJe Park and F. D. M. Haldane. Guiding-center hall viscosity and intrinsic dipole moment along edges of incompressible fractional quantum hall fluids. *Phys. Rev. B*, 90:045123, Jul 2014.

[35] Anthony Ralston and Philip Rabinowitz. *A first course in numerical analysis*. DOVER PUBLICATIONS, INC., 2001.

[36] N. Read. Non-abelian adiabatic statistics and hall viscosity in quantum hall states and $p_x + ip_y$ paired superfluids. *Phys. Rev. B*, 79:045308, Jan 2009.

[37] N. Read and E. Rezayi. Beyond paired quantum hall states: Parafermions and incompressible states in the first excited landau level. *Phys. Rev. B*, 59:8084–8092, Mar 1999.

[38] D. T. Son. Newton-cartan geometry and the quantum hall effect. arXiv:1306.0638, June 2013.

[39] D. J. Thouless, M. Kohmoto, M. P. Nightingale, and M. den Nijs. Quantized hall conductance in a two-dimensional periodic potential. *Phys. Rev. Lett.*, 49:405–408, Aug 1982.

[40] D. C. Tsui, H. L. Stormer, and A. C. Gossard. Two-dimensional magnetotransport in the extreme quantum limit. *Phys. Rev. Lett.*, 48:1559–1562, May 1982.

[41] Klaus von Klitzing. The quantized hall effect. *Rev. Mod. Phys.*, 58:519–531, Jul 1986.

[42] X. G. Wen. Theory of the edge states in fractional quantum hall effects. *Int. J. Mod. Phys. B*, 06:1711, 1992.

[43] X. G. Wen and A. Zee. Shift and spin vector: New topological quantum numbers for the hall fluids. *Phys. Rev. Lett.*, 69:953–956, Aug 1992.

[44] R. Willett, J. P. Eisenstein, H. L. Störmer, D. C. Tsui, A. C. Gossard, and J. H. English. Observation of an even-denominator quantum number in the fractional quantum hall effect. *Phys. Rev. Lett.*, 59:1776–1779, Oct 1987.

[45] Bo Yang, Zi-Xiang Hu, Z. Papić, and F. D. M. Haldane. Model wave functions for the collective modes and the magnetoroton theory of the fractional quantum hall effect. *Phys. Rev. Lett.*, 108:256807, Jun 2012.

[46] Bo Yang, Z. Papić, E. H. Rezayi, R. N. Bhatt, and F. D. M. Haldane. Band mass anisotropy and the intrinsic metric of fractional quantum hall systems. *Phys. Rev. B*, 85:165318, Apr 2012.

[47] Michael P. Zaletel and Roger S. K. Mong. Exact matrix product states for quantum hall wave functions. *Phys. Rev. B*, 86:245305, Dec 2012.